





Unraveling intricate magnetic behavior involving negative magnetization and exchange-bias in $\text{ErFe}_{0.5}\text{Co}_{0.5}\text{O}_3$

Deepak Garg , Amit Kumar , and S. M. Yusuf *

*Solid State Physics Division, Bhabha Atomic Research Centre, Mumbai 400085, India
and Homi Bhabha National Institute, Anushaktinagar, Mumbai 400094, India*

 (Received 9 March 2024; accepted 13 August 2024; published 3 September 2024)

In this paper, we present a comprehensive investigation of the distinctive magnetic properties involving the remarkable occurrences of negative magnetization (NM), exchange bias (EB), and spin reorientation (SR) in the $\text{ErFe}_{0.5}\text{Co}_{0.5}\text{O}_3$ compound. The dc magnetization data, recorded in field-cooled-cooling mode, reveal a net zero magnetization at the compensation temperature (T_{COMP}) of 24 K, leading to the NM phenomenon in the compound. Rietveld refinement of the neutron diffraction (ND) patterns over 1.5–300 K elucidates the SR of Fe/Co spins at 100 K (T_{SR}) and Er magnetic ordering <4 K (T_{N}^{Er}) resulting in $\Gamma_4(G_x)$, $\Gamma_{24}(G_z, G_x)$, $\Gamma_2(G_z)$, and $\Gamma_{257}(G_z; A_y^{\text{Er}} G_z^{\text{Er}})$ magnetic structures at $T > T_{\text{SR}}$, $T_{\text{SR}} \geq T > T_{\text{COMP}}$, $T_{\text{N}}^{\text{Er}} < T \leq T_{\text{COMP}}$, and $T \leq T_{\text{N}}^{\text{Er}}$, respectively. It is, therefore, evident that the SR of Fe/Co moments from $\Gamma_4(G_x)$ to $\Gamma_2(G_z)$ gets completed at the T_{COMP} of 24 K, and the Er magnetic ordering into an unusual $\Gamma_{57}(A_y^{\text{Er}} G_z^{\text{Er}})$ spin configuration takes place at $T \leq 4$ K. Anomalies in dc magnetization data (coercivity and remanent magnetization) at T_{SR} , T_{COMP} , and T_{N}^{Er} are also reflected in the ac susceptibility data. Intriguingly, EB field (H_{EB}) in the compound does not change its polarity across T_{COMP} and remains positive even above T_{COMP} . The observed positive H_{EB} at $T > T_{\text{COMP}}$ can be attributed to a complex spin arrangement as evident from the ND, whereas for $T \leq T_{\text{COMP}}$, positive H_{EB} has its usual explanation within the framework of the Meiklejohn-Beam model. The maximum positive H_{EB} and a broad hump in H_{EB} at T_{COMP} and T_{SR} , respectively, indicate a correlation between the EB and SR in the compound. Additionally, cooling-field dependence of the EB shows a peak value ~ 5 kOe; thereafter, an unusual suppression of H_{EB} up to 70 kOe cooling field is found. The observed NM below T_{COMP} is elucidated using the Cooke's model, where the polarized Er moment, under the internal magnetic field of the ordered canted antiferromagnetic Fe/Co sublattice, competes with the ferromagnetic Fe/Co moment. This results in a complete cancellation of magnetization at T_{COMP} and the emergence of NM below T_{COMP} in the compound. The specific heat data reveal a Schottky anomaly, inferring the dominant polarized nature of the Er moment below T_{COMP} . In this paper, we underscore the pivotal role of Er and Fe/Co exchange coupling in shaping the intriguing and complex magnetic properties—NM and EB—of the compound. These findings highlight the potential utility of the compound in spintronic applications.

DOI: [10.1103/PhysRevB.110.104401](https://doi.org/10.1103/PhysRevB.110.104401)

I. INTRODUCTION

The negative magnetization (NM) or magnetization-reversal phenomenon [1,2], wherein the dc magnetization becomes negative below a compensation temperature (T_{COMP}) while cooling the compound under a constant and positive external magnetic field, has become an interesting topic of research lately from the fundamental and applications points of view. The possibility of tuning magnetization signs with changing temperature involving a zero value of magnetization at T_{COMP} makes the NM compounds potential materials for thermomagnetic switches and spin-resolving devices [2]. Exchange bias (EB) [3,4], on the other hand, is another magnetic phenomenon that has implications in high-density magnetic storage [5] and voltage-mediated magnetic switching devices [6]. EB is manifested as the shifting of the hysteresis loop when the compound is cooled under an external magnetic field. Since its discovery [7], various heterogeneous systems having ferromagnetic (FM)/antiferromagnetic (AFM)

[8], FM/FM [9], and AFM/spin-glass [10] interfaces have been reported to show EB. In recent years, attention has been given to studying EB in homogeneous systems exhibiting NM which, unlike the heterogeneous systems discussed above, do not have any clear interface. In this direction, various homogeneous systems like orthochromites [11–14], spinels [15,16], manganites [17,18], and the intermetallic compounds [19,20] have been studied by various researchers. Moreover, NM and EB studies in orthoferrites $R\text{FeO}_3$ (R is rare-earth) have also been reported in the literature [21,22].

The $R\text{FeO}_3$ compounds crystallize in the orthorhombic crystal structure (space group: $Pbnm$ or $Pnma$) and have importance in magnetic memories [23] and multiferroic-based applications [24,25]. In these compounds, Fe spins magnetically order at high Néel temperature ($T_{\text{N}} \sim 650\text{--}740$ K) into G -type AFM spin configuration with a weak FM component (F) perpendicular to the AFM spins [26]. The weak FM component arises from the canting of AFM-ordered Fe spins due to the Dzyaloshinskii-Moriya exchange interaction [27,28]. Further, the antisymmetric and anisotropic-symmetric exchange interactions [29] between the R and Fe spins lead to

*Contact author: smyusuf@barc.gov.in

the temperature-induced spin-reorientation (SR) transition in these compounds, except for $R = \text{La, Eu, Gd, Lu, and Y}$ [26]. The SR is continuous except for $R = \text{Dy}$, where abrupt SR has been reported [26]. In the continuous SR transition, Fe spins gradually rotate from one direction to another below the SR transition temperature, leading to a change in magnetic spin configuration, e.g., $G_x F_z$ to $G_z F_x$ ($Pbnm$ space group). Here, $G_x F_z$ ($G_z F_x$) represents the ordering of Fe spins in G -type AFM configuration along the x (z) axis with a FM component along the z (x) axis. On the other hand, Fe spins abruptly rotate from $G_x F_z$ to G_y in the abrupt SR [26]. In $R\text{FeO}_3$ compounds with $R = \text{Nd, Sm, and Er}$, NM along with EB have been reported [21,22,30]. NdFeO_3 and ErFeO_3 show the EB reversal across their T_{COMP} (~ 9.2 K for Nd and ~ 45 K for Er) with maximum EB at T_{COMP} . The sign reversal of EB across T_{COMP} (~ 4 K) is also reported for the SmFeO_3 compound; however, the compound shows zero EB at T_{COMP} . In doped $R\text{FeO}_3$ compounds such as $\text{LuFe}_{0.5}\text{Cr}_{0.5}\text{O}_3$ [31], $\text{NdFe}_{0.5}\text{Cr}_{0.5}\text{O}_3$ [32], and $\text{YbCr}_{1-x}\text{Fe}_x\text{O}_3$ [33], NM and EB have also been studied. $\text{LuFe}_{0.5}\text{Cr}_{0.5}\text{O}_3$ and $\text{NdFe}_{0.5}\text{Cr}_{0.5}\text{O}_3$ compounds show EB behavior like SmFeO_3 , though an anomalous EB without any sign reversal around the SR has been reported for $\text{YbCr}_{1-x}\text{Fe}_x\text{O}_3$. These studies indicate the different kinds of EB behaviors in parent and doped orthoferite compounds. Further, the unusual magnetic properties viz. complex magnetic ordering and metamagnetic and successive SR have been reported in other doped $R\text{FeO}_3$ compounds like $\text{NdFe}_{0.5}\text{Mn}_{0.5}\text{O}_3$ [34], $(\text{Pr}_{0.5}/\text{Nd}_{0.5}/\text{Er}_{0.5})\text{Dy}_{0.5}\text{FeO}_3$ [35–37], and $(\text{Tb}/\text{Dy}/\text{Ho}/\text{Er})\text{Fe}_{0.5}\text{Cr}_{0.5}\text{O}_3$ [38]. However, such studies, namely NM, EB, SR, and magnetic ordering, in Co-doped $R\text{FeO}_3$ compounds are lacking so far in the literature. Moreover, a correlation between EB and SR in NM compounds has also not been explored much in the literature. Interest arises in Co^{3+} doping mainly due to its various spin-states, i.e., low spin ($S = 0$; $t_{2g}^6 e_g^0$), intermediate spin ($S = 1$; $t_{2g}^5 e_g^1$), and high spin ($S = 2$; $t_{2g}^4 e_g^2$). In $R\text{CoO}_3$, Co^{3+} remains in a low-spin (nonmagnetic) state up to 300 K [39,40]. Above room temperature, it exhibits spin-state transitions leading to intermediate- and high-spin states [41]. In this paper, we aim to study the $\text{ErFe}_{0.5}\text{Co}_{0.5}\text{O}_3$ (EFCO) compound, where replacement of Co at Fe sites modifies the Fe-Fe and R-Fe superexchange interactions, which in turn could give intriguing and complex magnetism in the EFCO compound.

In a preliminary study on the EFCO compound, Lohr *et al.* [42] showed the presence of the NM phenomenon in the compound, and neutron diffraction (ND) was performed only at 300, 60, and 2 K, inferring $\Gamma_4(G_x)$, $\Gamma_{24}(G_z, G_x)$ and $\Gamma_{25}(G_z; G_x^{\text{Er}} A_y^{\text{Er}})$ magnetic structures, respectively. However, the physics understanding of NM and EB and detailed knowledge of the magnetic structures/magnetic moments of the EFCO compound using dc magnetization, ac susceptibility, neutron depolarization, specific heat, and ND techniques are reported in this paper.

Our dc magnetization data reveal the NM phenomenon with T_{COMP} of 24 K in the EFCO compound. Remarkably, in this paper, we show an unusual EB with the maximum (positive) H_{EB} at $T = T_{\text{COMP}}$, and H_{EB} remains positive even for $T \geq T_{\text{COMP}}$ in the compound. This H_{EB} behavior is different in comparison with other NM compounds, showing zero H_{EB} at

T_{COMP} and negative H_{EB} above T_{COMP} [11,12,30–32,43]. The observed unusual EB is attributed to the complex arrangement of Fe/Co spins, as evident from the ND. In this paper, we also reveal a correlation between EB and SR. A nonmonotonic H_{EB} with cooling magnetic field is also observed. Interestingly, an unusual magnetic ordering of Er at $T_{\text{N}}^{\text{Er}} \sim 4$ K into $\Gamma_{57}(A_y, G_z)$ spin configuration is found in this paper. The polarized nature of Er (evident from specific heat and ac susceptibility) under the internal field of Fe/Co is understood to be responsible for the NM phenomenon in the compound. The observed unusual behavior of magnetization (NM) and EB makes the EFCO compound useful for various spintronic applications.

II. EXPERIMENTAL DETAILS

The polycrystalline EFCO compound was prepared by the conventional solid-state reaction method. The stoichiometric ratio of the high-purity ($>99.9\%$) starting chemicals Er_2O_3 , Fe_2O_3 , and Co_3O_4 was mixed in an agate mortar and pestle for 8 h. The resulting mixture was sintered in a Carbolite furnace at 750, 850, and 900 °C for 24 h each; then the furnace was allowed to cool down to room temperature. The reacted product was ground again and sintered at 1000 °C for 30 h with various intermediate grindings.

X-ray diffraction was performed using $\text{Cu } K\alpha$ radiation for phase identification of the compound. Energy-dispersive x-ray spectroscopy (EDX; Carl Zeiss, GEMINISEM 300) was used to study the elemental composition of the compound. The dc magnetization (M) measurements were carried out in field-cooled-cooling (FCC) and zero-field-cooling (ZFC) modes over a temperature (T) range of 3–310 K under various magnetic fields (H) using a commercial vibrating sample magnetometer. The ac susceptibility was measured over a T range of 7–310 K under 987 Hz frequency using a commercial ac susceptibility setup. Isothermal $M(H)$ hysteresis loops were recorded in ZFC/field-cooled (FC) modes. For FC $M(H)$ loops, the compound was first cooled from 310 K to the measurement T under a finite H , and thereafter the $M(H)$ loop was recorded in a H range of ± 50 kOe, whereas the ZFC $M(H)$ loops were recorded after cooling the compound under zero magnetic field. The specific heat measurements were carried out on a pellet of the EFCO sample over a T range of 1.8–305 K under various H using a Quantum Design Physical Property Measurement System. The neutron depolarization experiment ($\lambda = 1.201$ Å) was carried out using the polarized neutron spectrometer at Dhruva reactor, BARC, Mumbai, India. To study the thermal evolution of the sublattice magnetic moments and the magnetic structure of the compound, the ND patterns were recorded at various temperatures under zero H using position-sensitive-detector-based powder diffractometers viz. PD-1 ($\lambda = 1.094$ Å) and PD-2 ($\lambda = 1.2443$ Å) at Dhruva reactor, BARC, Mumbai, India. All (x-ray and neutron) diffraction patterns were analyzed using the Rietveld refinement [44] implemented in the FULLPROF software [45].

III. RESULTS AND DISCUSSION

A. Structural characterization

Figure 1(a) shows the Rietveld refined [44] x-ray diffraction pattern of EFCO compound at 300 K. The refinement

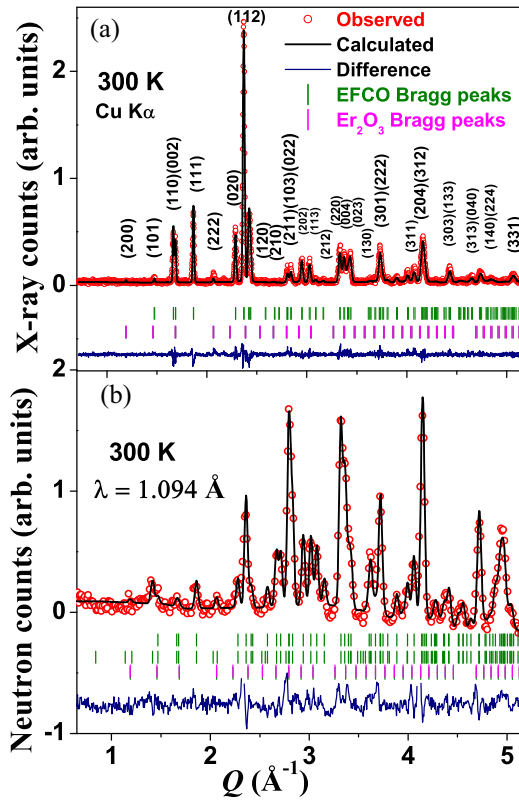


FIG. 1. Rietveld refined (a) x-ray (Cu $K\alpha$) and (b) neutron diffraction ($\lambda = 1.094 \text{ \AA}$) patterns of the EFCO compound at 300 K. Here, the x axis corresponds to momentum transfer, $|Q| = 4\pi(\sin\theta)/\lambda$, where λ is the wavelength of the x-ray/neutron, and θ is the Bragg angle. The experimental data are shown by open symbols (red color), whereas the black line represents the calculated pattern. The vertical lines represent the positions of the Bragg peaks of EFCO (olive) and Er_2O_3 (pink) phases, respectively. The difference between the experimental and calculated data is shown by navy blue line at the bottom of each fitted data.

reveals that the compound crystallizes in the orthorhombic crystal structure ($Pbnm$ space group), and the derived lattice constants are $a = 5.194$ (1) \AA , $b = 5.500$ (2) \AA , and $c = 7.459$ (1) \AA , which are close to the literature reported values [42]. The refinement has also revealed a small (~ 2 vol. %) phase fraction of the Er_2O_3 (space group: $Ia-3$) in the present compound [vertical pink lines in Fig. 1(a)]. This small R_2O_3 phase was also reported in RFCO ($R = \text{Ho, Tb, Er, Dy, and Tm}$) compounds [42]. Since the EFCO compound consists of neighboring Fe and Co and lighter O elements, x-ray diffraction is not very effective in determining the occupation number of Fe/Co and the atomic coordinates of the O atoms. In this regard, ND is advantageous, as the coherent neutron scattering lengths of Fe ~ 9.45 fm and Co ~ 2.49 fm are quite different from each other, and the O scattering length (~ 5.8 fm) is also large. The Rietveld refined ND pattern ($\lambda = 1.094 \text{ \AA}$) of the present EFCO compound at 300 K is shown in Fig. 1(b). The derived chemical composition of the compound is $\text{ErFe}_{0.46}\text{Co}_{0.54}\text{O}_3$, and the refined structural parameters are listed in Table S1 in Supplemental Material (SM) [46]. The Rietveld refinement of the ND data reveals a

random distribution of $\text{Fe}^{3+}/\text{Co}^{3+}$ ions at the $4b$ site without any clustering. Further, as shown in Fig. 1(b), the (011) Bragg reflection at $Q = 1.42 \text{ \AA}^{-1}$ is not indexed in the $Pbnm$ space group, indicating that the compound is magnetic at 300 K. Therefore, the magnetic phase has been added in the analysis of ND data [middle set of vertical lines at the bottom in Fig. 1(b)], details of which are given later (Sec. III B 3).

The EDX spectrum (Fig. S1 in the SM [46]) confirms the presence of Er, Fe, Co, and O atoms in the EFCO compound, and the EDX estimated atomic ratios (Table S2 in the SM [46]) are in good agreement with that from the ND [46].

B. Magnetic study

1. dc magnetization and ac susceptibility

The $M(T)$ curves measured in the ZFC and FCC modes under an applied magnetic field of 100 Oe are depicted in Fig. 2(a). It is evident that, with a decrease in temperature from 310 K, magnetization in both measurement modes increases down to $T \sim 100$ K. In the literature, this temperature is denoted as the SR transition [42]. At $T < 100$ K, magnetization in the ZFC mode starts to decrease, whereas it still increases in the FCC mode down to ~ 50 K. With a further decrease in temperature, the FCC magnetization curve shows a downturn, crossing the ZFC curve at $T \sim 34$ K, and then becomes zero at a compensation temperature (T_{COMP}) of 24 K. At $T < T_{\text{COMP}}$, the FCC magnetization becomes negative, and it remains negative down to the lowest measured temperature (3 K), whereas the magnetization remains positive in the ZFC mode in the whole measured temperature range. A kink is also observed at $T \sim 4$ K in both ZFC and FCC magnetization curves [inset of Fig. 2(a)], indicating a magnetic transition at low temperature. To get more details about the NM in the EFCO compound, the dc magnetization data have been recorded in the FCC mode under various magnetic fields, and the results are displayed in Fig. 2(b). It is evident that the compound shows the NM phenomenon up to $H = 450$ Oe with T_{COMP} decreasing with increasing H [inset of Fig. 2(b)]. The T_{COMP} 's are also calculated using the Cooke's model (discussed later), and good agreement is found with the experimental T_{COMP} 's. For $H > 450$ Oe, the dc magnetization remains positive throughout the measured temperature range; however, a sharp upturn in magnetization is observed for $H \geq 1$ kOe. Figure 2(c) shows the temperature dependence (7–310 K) of the ac susceptibility under a frequency of 987 Hz. An anomaly at $T \sim T_{\text{COMP}}$ [main panel of Fig. 2(c)] and a small kink at ~ 100 K [shown by an arrow in the inset of Fig. 2(c)] are clearly visible in the ac susceptibility data. However, the magnetic transition at $T \sim 4$ K could not be captured due to the limitation of the restricted temperature range. No signature of onset of magnetic ordering is found in measured dc/ac magnetization data, indicating that the magnetic ordering sets in the compound at $T > 310$ K.

In brief, the dc magnetization data, i.e., ZFC and FCC $M(T)$, reveal anomalies at various temperatures viz. $T \sim 100$ K, T_{COMP} (24 K), and 4 K. Magnetic anomalies at T_{COMP} and 100 K are also visible in the ac susceptibility data. Interesting features across these temperatures are also observed in the thermal variations of hysteresis loop parameters viz. H_C ;

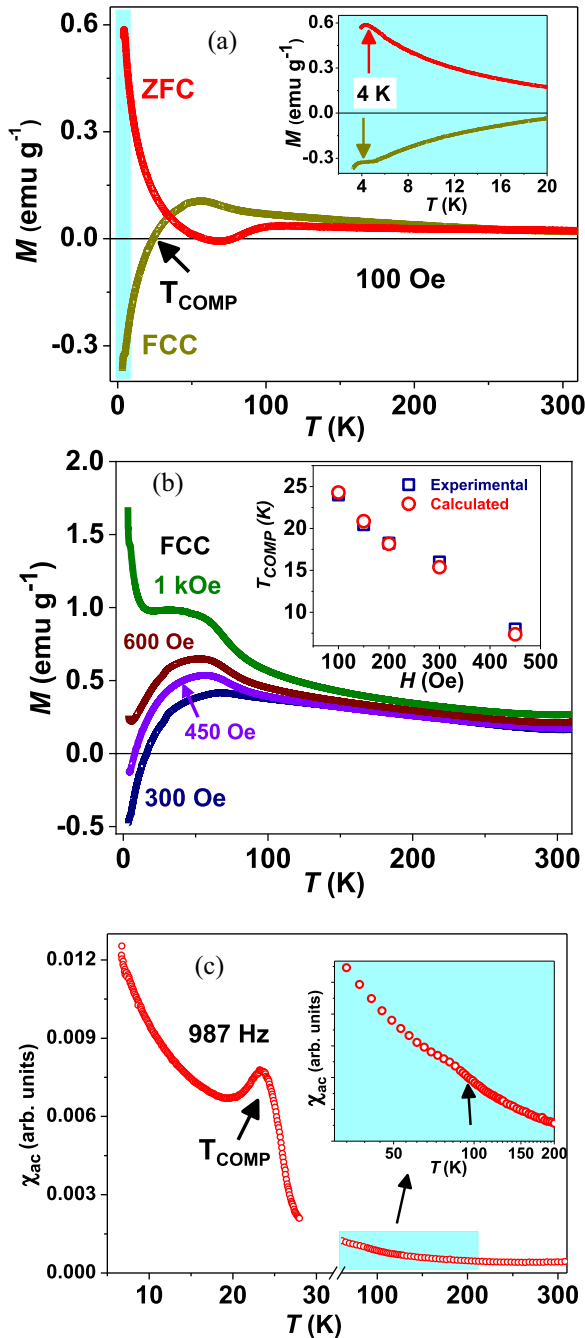


FIG. 2. (a) The zero-field-cooling (ZFC, red) and field-cooled-cooling (FCC, dark yellow) $M(T)$ curves of the EFCO compound under $H = 100$ Oe. Inset shows the enlarged view of the highlighted area showing a kink at $T \sim 4$ K. (b) FCC $M(T)$ curves under various cooling fields. Inset shows the variation of experimental (square) and calculated (circle) T_{COMP} with H . (c) Temperature dependence of the ac susceptibility (χ_{ac}) showing anomaly at $T \sim T_{\text{COMP}}$ (main panel) and a small kink at ~ 100 K (inset) under 987 Hz.

coercivity, M_{R} ; remanent magnetization, H_{EB} ; horizontal shift and M_{EB} ; vertical shift (discussed later). To get an in-depth understanding of these anomalies, temperature-dependent neutron depolarization (mesoscopic technique) and ND (microscopic technique) experiments have been performed. The results are discussed in the next sections.

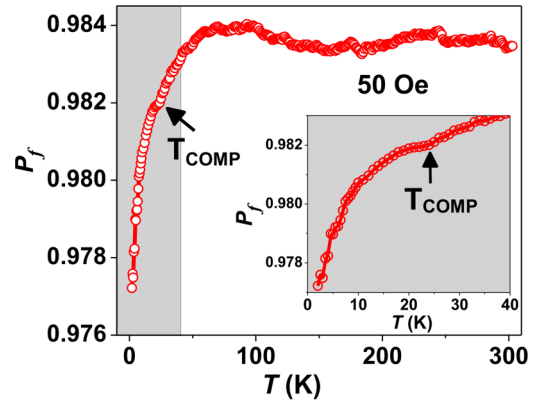


FIG. 3. Temperature dependence of the transmitted neutron beam polarization (P_f) of the EFCO compound measured under $H = 50$ Oe. Inset shows the enlarged view of the shaded region of the curve depicting the slope change at $T = T_{\text{COMP}}$ and a sharp fall < 4 K.

2. Neutron depolarization

The neutron depolarization experiment provides the mesoscopic understanding of the magnetic behavior of the sample at a length scale of 100 \AA to several micrometers [47–49]. In this experiment, a polarized neutron beam is allowed to pass through the sample, and the polarization of the transmitted beam (P_f) is analyzed. During this passage from the ferromagnetic/ferrimagnetic/canted AFM compound with a net magnetization, the polarized beam gets depolarized owing to the Larmor precession from the local magnetic field of domains. However, no depolarization of the neutron beam is expected from the paramagnetic, collinear AFM, and canonical spin-glass systems having average zero magnetization at the mesoscopic lengths scales. Thus, the neutron depolarization experiment provides a good estimate of domain-magnetization/size variation with the temperature of the sample under study.

Figure 3 shows P_f as a function of temperature (2–300 K) under $H = 50$ Oe for the EFCO compound. A finite depolarization is observed mainly < 100 K, and it increases with decreasing temperature followed by a clear change in slope at T_{COMP} (24 K) and a sharp fall of P_f below 4 K [inset of Fig. 3]. Surprisingly, a full recovery of the neutron beam polarization is not observed at T_{COMP} , which is in contrast with other NM compounds, such as YbCrO_3 [12], DyFe_5Al_7 [50], and $\text{Li}_{0.5}\text{FeCr}_{1.5}\text{O}_4$ [51], where a full recovery of the neutron beam polarization at T_{COMP} was reported. It may be noted that, for these reported compounds, the magnetic structure does not change across T_{COMP} . Further, an incomplete recovery of the neutron beam polarization at T_{COMP} was reported for the NM compound NdMnO_3 [52]. In NdMnO_3 , an isostructural to the present EFCO compound, a change in the magnetic structure was reported at T_{COMP} , involving a simultaneous reorientation of the Mn spins by 180° and the Nd sublattice ordering. These facts indicate that the observed neutron depolarization behavior (Fig. 3) of the present EFCO compound could be due to the complex magnetic structural changes across T_{COMP} , which is further needed to be understood. Temperature-dependent ND experiments (discussed in the next section) are

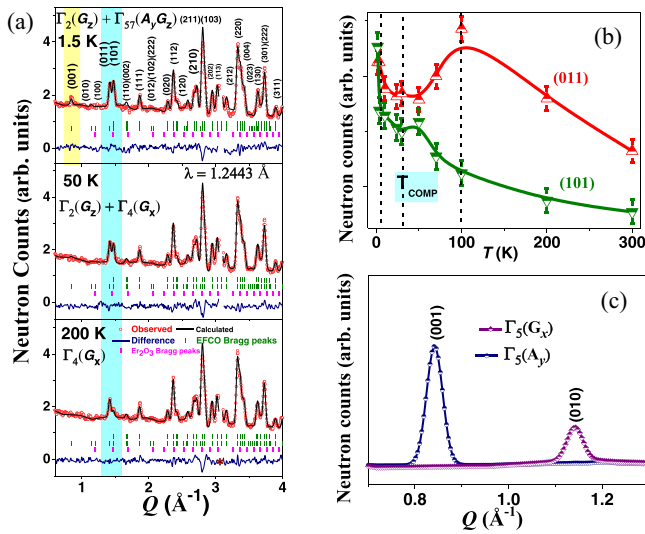


FIG. 4. (a) Rietveld-refined neutron diffraction patterns at some of the selected temperatures. Magnetic Bragg peaks are highlighted by colored (yellow and cyan) areas. The observed and calculated data are shown by open symbols (red) and line (black), respectively. The difference pattern is shown at the bottom of each curve by the navy blue line. The vertical lines (olive) represent the positions of nuclear and magnetic Bragg peaks of the EFCO compound, whereas the pink lines correspond to the nuclear Bragg peaks of the Er_2O_3 compound. The star indicates the excluded peak coming from the cryostat. (b) Thermal variations of the intensities of (011) and (101) Bragg peaks. (c) Simulated Bragg peaks corresponding to G_x and A_y configurations of Er spins in the Γ_5 representation.

carried out on the compound to shed light on this intriguing neutron depolarization behavior.

3. Temperature-dependent ND

The Rietveld refined ND patterns of the EFCO compound at some of the selected temperatures are shown in Fig. 4(a). The (011) Bragg peak at $Q = 1.42 \text{\AA}^{-1}$ is forbidden in the $Pbnm$ space group. This Bragg peak is purely magnetic, whereas the (101) Bragg peak at $Q = 1.47 \text{\AA}^{-1}$ has some nuclear contribution as well. The temperature-dependent variation in the intensities of these two Bragg peaks are shown in Fig. 4(b). The intensities of the (011) and (101) Bragg peaks increase with a decrease in temperature down to 100 K, a characteristic temperature below which the ZFC and FCC magnetization curves show opposite behaviors [Fig. 2(a)], and the ac susceptibility data show a small kink [inset of Fig. 2(c)]. Below 100 K, the intensity of the (011) Bragg peak decreases, while that of the (101) Bragg peak still increases. Such a variation of the integrated intensities of (011) and (101) Bragg peaks indicates the onset of SR transition in the compound, as reported for similar $R_{0.5}\text{Dy}_{0.5}\text{FeO}_3$ ($R = \text{Nd}$ and Er) [35,37] and SmCrO_3 [53] compounds. This contrasting behavior of (011) and (101) Bragg peak intensities persists down to 50 K, a temperature at which a maximum positive dc magnetization is observed in the FCC mode [Fig. 2(a)]. Below 50 K, the intensity of the (011) Bragg peak increases with lowering of temperature down to 1.5 K, while a sharp rise

in the (101) Bragg peak intensity is observed < 4 K. Moreover, a new Bragg peak (001) at $Q = 0.84 \text{\AA}^{-1}$ is observed < 4 K [Fig. 4(a)]. The complex temperature variations of (011) and (101) Bragg peaks and the appearance of the (001) Bragg peak indicate the multiple magnetic structures/transitions in the EFCO compound that are discussed in the next paragraph.

In the RFeO_3 compounds, Fe ions occupy the $4b$ crystallographic site at positions $(\frac{1}{2}, 0, 0)$, $(\frac{1}{2}, 0, \frac{1}{2})$, $(0, \frac{1}{2}, \frac{1}{2})$, and $(0, \frac{1}{2}, 0)$, and the corresponding magnetic irreducible representations (IRs) in the Bertaut notation [54] are $\Gamma_1(A_x, G_y, C_z)$, $\Gamma_2(F_x, C_y, G_z)$, $\Gamma_3(C_x, F_y, A_z)$, and $\Gamma_4(G_x, A_y, F_z)$. On the other hand, the R ions occupy the $4c$ crystallographic site at positions $(x, y, \frac{1}{4})$, $(-x, -y, \frac{3}{4})$, $(x + \frac{1}{2}, -y + \frac{1}{2}, \frac{3}{4})$, and $(-x + \frac{1}{2}, y + \frac{1}{2}, \frac{1}{4})$. The associated IRs are $\Gamma_1(C_z)$, $\Gamma_2(F_x, C_y)$, $\Gamma_3(C_x, F_y)$, $\Gamma_4(F_z)$, $\Gamma_5(G_x, A_y)$, $\Gamma_6(A_z)$, $\Gamma_7(G_z)$, and $\Gamma_8(A_x, G_y)$. The Rietveld refinement of the ND patterns in the temperature range of $100 \text{ K} < T \leq 300 \text{ K}$ shows that the ND data are fitted well with the $\Gamma_4(G_x, A_y, F_z)$ with G_x -type AFM ordering of Fe/Co spins. At $T \leq 100$ K, the ND data do not fit with only G_x -type ordering of Fe/Co spins; therefore, we have tried other magnetic models allowed by the representation analysis to fit the observed ND data. Good agreement has been obtained between the experimental and calculated ND data in the temperature range of $T_{\text{COMP}} < T \leq 100$ K using a mixture of AFM $G_x(\Gamma_4)$ and $G_z(\Gamma_2)$ components of Fe/Co spins. For instance, at 50 K, a lower value of magnetic profile factor ($R_{\text{mag}} \sim 12.2$) is obtained using both $G_x(\Gamma_4)$ and $G_z(\Gamma_2)$ in comparison with the higher $R_{\text{mag}} \sim 18.8$ and 13.4 obtained using $G_x(\Gamma_4)$ and $G_z(\Gamma_2)$, respectively. The analysis of ND data, therefore, indicates the onset of temperature-induced SR transition at 100 K, where the AFM Fe/Co moments start to rotate from the x to the z axis. This SR occurs continuously down to T_{COMP} , where the AFM Fe/Co moments rotate completely along the z axis. In the temperature range of $1.5 < T \leq T_{\text{COMP}}$, only the $G_z(\Gamma_2)$ -type AFM configuration of Fe/Co moments gives good agreement between the experimental and calculated ND data. Further, in the literature, the (001) Bragg peak is attributed to the Er ordering in $\Gamma_5(G_x, A_y)$ with both components $G_x = 0.65(6) \mu_B$ and $A_y = 0.77(6) \mu_B$ [42]. In this paper, the contributions of these two components (G_x and A_y), corresponding to Γ_5 , to various Bragg peaks are simulated using the FULLPROF software [45]. The simulated patterns reveal that the A_y component of Γ_5 should give finite intensity to the (001) Bragg peak, while G_x should contribute to the intensity of the (010) Bragg peak [Fig. 4(c)]. However, no (010) Bragg peak positioned at $Q = 1.14 \text{\AA}^{-1}$ is found in the present ND data [Fig. 4(a)]. Thus, the Rietveld refinement of the ND data at 1.5 K has been carried out by considering the $A_y(\Gamma_5)$ component for Er moments, and good agreement between the observed and calculated data has been obtained [Fig. 4(a)]. The $\Gamma_5(G_x, A_y)$ corresponding to Er spins with $G_x = 0 \mu_B$ and $A_y = 0.75(1) \mu_B$ accounts only for the intensity of the (001) Bragg peak but does not account for the sudden increase of the (101) Bragg peak intensity < 4 K. This increase is accounted by adding $\Gamma_7(G_z)$ of Er spins in the Rietveld refinement of the ND data at 1.5 K with $G_z = 1.42(2) \mu_B$. The result is consistent with the literature report on the DyFeO_3 compound [55], where the enhanced intensity of the (101) Bragg peak is accounted by $\Gamma_7(G_z)$ IR of Dy. Thus, the

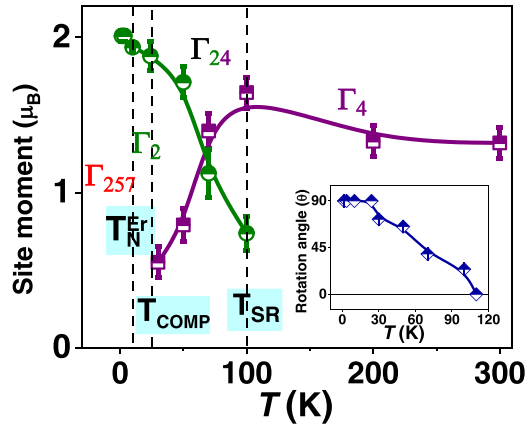


FIG. 5. Temperature variations of the antiferromagnetic (AFM) Fe/Co magnetic moment in $\Gamma_4(G_x)$ (half-filled square symbols, purple color) and $\Gamma_2(G_z)$ (half-filled circular symbols, olive color) configurations. The details about the Γ_4 , Γ_{24} , Γ_2 , and Γ_{257} configurations over different temperature ranges are given in the text. Inset shows the variation of rotation angle of AFM Fe/Co magnetic moment with temperature.

magnetic moment components of Er at 1.5 K are $G_x = 0 \mu_B$, $A_y = 0.75 (1) \mu_B$, and $G_z = 1.42 (2) \mu_B$ corresponding to Γ_{57} . The average magnetic moment ($\sim 2 \mu_B$ at 1.5 K) at the $4b$ site indicates that Co^{3+} ions are in the low-spin state ($S = 0$), as discussed in the Introduction [39,40]. Here, we mention that all magnetic Bragg peaks are indexed with the $k = [0, 0, 0]$ propagation vector, consistent with the Lohr *et al.* [42] study on the EFCO compound. The other crystallographic parameters derived from the Rietveld refinement of the ND data at 1.5 K are listed in Table S1 in the SM [46].

Now we compare the magnetic structure of the EFCO compound with ErFeO_3 and other orthoferrite compounds. The derived $G_x(\Gamma_4)$ and $G_z(\Gamma_2)$ magnetic structures for the present EFCO compound match well with the reported magnetic structures for ErFeO_3 [56] and are in agreement with the other orthoferrite compounds [26,35,37]. However, the temperature-induced SR process spreads over 24–100 K in EFCO as compared with a narrow range of 100–110 K in ErFeO_3 . This may be attributed to the modification of Er-Fe exchange-coupling because of Co substitution at Fe sites in

the EFCO compound. On the other hand, the Er magnetic ordering in $\Gamma_{57}(A_y G_z)$ in the present EFCO compound is different as compared with the reported $\Gamma_1(C_z)$ of Er in ErFeO_3 [56] and $\Gamma_2(F_x C_y)$ for other $R\text{FeO}_3$ ($R = \text{Nd, Sm, and Ho}$) compounds [26,57,58]. Further discussion about the unusual Er ordering in the present EFCO compound is given later.

The temperature variations of the AFM $G_x(\Gamma_4)$ and $G_z(\Gamma_2)$ moments of the Fe/Co spins in the present EFCO compound are shown in Fig. 5. At 300 K, the derived AFM G_x moment is $\sim 1.25 \mu_B$, which is close to the reported value of $0.98 \mu_B$ by Lohr *et al.* [42]. It increases monotonically with decreasing temperature down to 100 K (T_{SR}), where Fe/Co SR starts. With the onset of SR, the G_x moment starts to decrease, whereas the AFM G_z shows an increase. At $T \sim T_{\text{COMP}}$, the AFM Fe/Co moments are completely oriented along the z direction (G_z), and no moment corresponding to G_x is observed. We have estimated the rotation angle (θ) as a function of temperature using the AFM G_x and G_z components of the Fe/Co moment as $\theta = \arctan(G_z/G_x)$, and the plot of the rotation angle is shown in the inset of Fig. 5. The rotation angle first increases with decreasing temperature, reaches to 90° (complete SR), and then sustains this value down to 1.5 K (the lowest temperature in the present ND study). The different magnetic structures of the EFCO compound over different temperature ranges are shown in Fig. 6. Here, we mention that the observed $T_{\text{COMP}} = 24$ K (T_{SR2}) and $T_{\text{SR}} = 100$ K (T_{SR1}) of the EFCO compound prepared by the solid-state reaction method do not match with the values 9 K (T_{COMP}), 15 K (T_{SR2}), and 80 K (T_{SR1}), respectively, for the EFCO compound prepared by the thermal decomposition method as reported by Lohr *et al.* [42]. Here, T_{SR1} and T_{SR2} denote the onset and completion of SR transition, respectively. It is known that NM and SR phenomena are attributed to the magnetic anisotropy energy [1,26], which is strongly affected by various factors, such as strain, grain size, and shape formed during sample preparation. As different preparation methods for the EFCO compound are used in both studies (this paper and Ref. [42]), therefore, the differences in T_{COMP} and SR temperatures for the EFCO compound may be attributed to the strain/grain-size/shape effects [56]. The different T_{COMP} and SR temperatures (T_{SR1} and T_{SR2}) are also reported in the literature for the ErFeO_3 compound, as shown in Table I.

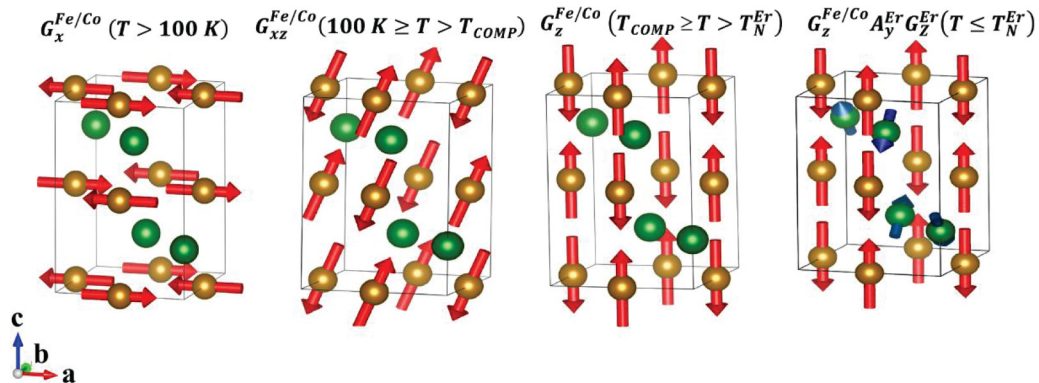


FIG. 6. Magnetic structures of the EFCO compound derived from the neutron diffraction study in different temperature regions. Here, golden- and olive-colored spheres represent the Fe/Co and Er ions, respectively. Oxygens ions are omitted for clarity.

TABLE I. Comparisons of the T_{COMP} , T_{SR1} (onset of SR), and T_{SR2} (complete SR) for ErFeO_3 and $\text{ErFe}_{0.5}\text{Co}_{0.5}\text{O}_3$ compounds.

Compound	T_{COMP} (K)	T_{SR1} (K)	T_{SR2} (K)	Synthesis technique	Refs.
ErFeO_3	45	110	100	Solid-state reaction	[56]
ErFeO_3	^a	105	88	^a	[59]
ErFeO_3	38	93	76	Hydrothermal synthesis	[60]
ErFeO_3	48	98	85	Coprecipitation	[61]
$\text{ErFe}_{0.5}\text{Co}_{0.5}\text{O}_3$	9	80	15	Thermal decomposition	[42]
$\text{ErFe}_{0.5}\text{Co}_{0.5}\text{O}_3$	24	100	24	Solid-state reaction	This paper

^aNot reported.

The variations of derived lattice parameters and the unit-cell volume with temperature are shown in Fig. 7. It is evident that lattice parameters a and c decrease monotonically with temperature down to 1.5 K except for a slight increase around T_{COMP} . On the other hand, the lattice parameter b first decreases down to 50 K, and thereafter, it increases, thus showing the negative thermal expansion of the unit cell along the b direction. The negative thermal expansion in the SR region is also reported in other related compounds [35,57]. The unit-cell volume V varies similarly to a and c and shows an insignificant magnetoelastic or magnetovolume effect due to SR.

In brief, our ND study has provided a microscopic understanding of the magnetic transitions observed in dc magnetization and ac susceptibility measurements. These transitions are identified as onset of SR at 100 K, completion of SR at T_{COMP} , and magnetic ordering of Er spins at ~ 4 K. We, therefore, assign 100 and 4 K temperatures as T_{SR} and T_{N}^{Er} , respectively, for the rest of this paper.

4. Specific heat

Figure 8(a) shows the specific heat (C_p) data of the EFCO compound over a temperature range of 1.8–305 K under zero magnetic field. It is evident that, with decreasing temperature, C_p decreases monotonically down to 8 K; thereafter, it increases and shows an anomaly at 3 K [inset of Fig. 8(a)]. The C_p anomaly is close to the magnetic ordering

temperature of Er spins. Further, the zero-field C_p data do not show any marked signatures of SR transitions at 24 and 100 K. It should be noted that C_p at high temperature (305 K) is $123.7 \text{ J mol}^{-1} \text{ K}^{-1}$, which is close to the expected value of $124.7 \text{ J mol}^{-1} \text{ K}^{-1}$ as per the Dulong-Petit law [62], indicating good C_p data and quality of our sample.

To determine the nature of the observed anomaly at low temperature, C_p data have been recorded over a temperature range of 1.8–30 K under various magnetic fields [Fig. 8(b)]. The C_p data under magnetic fields show behavior like that of the zero-field data; however, the anomaly becomes broad and shifts toward higher temperature with increasing magnetic field. This kind of behavior of the C_p anomaly is a signature of the Schottky anomaly. Therefore, the present C_p data under zero and finite magnetic fields are fitted by considering the two-level Schottky term along with the phononic terms using

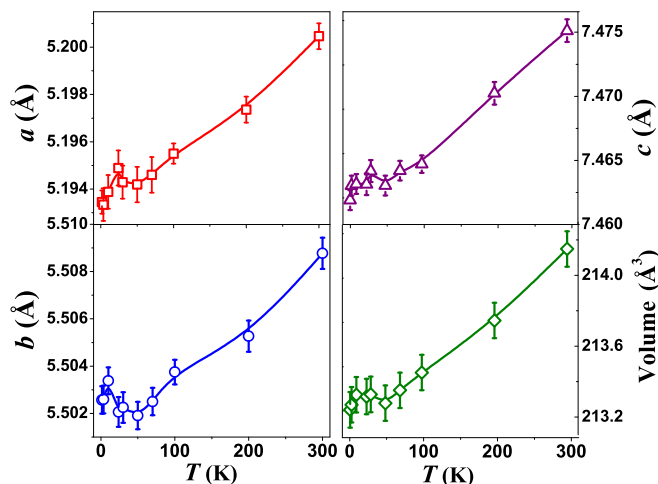


FIG. 7. Thermal variations of lattice parameters (a , b , and c) and unit-cell volume of the EFCO compound.

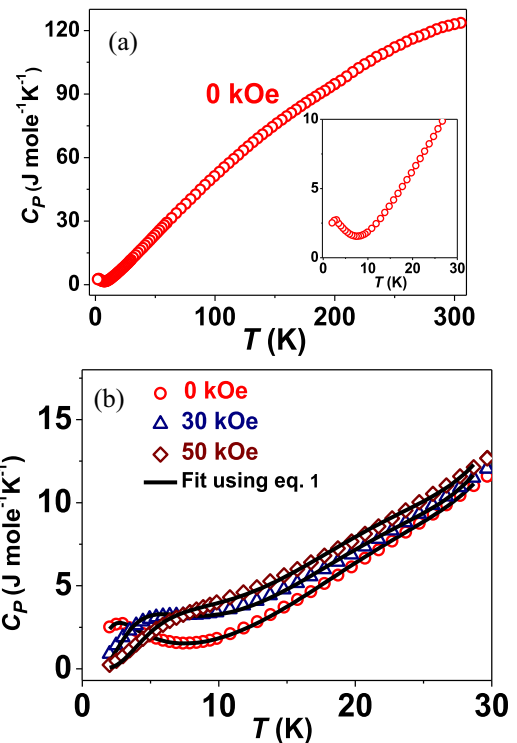


FIG. 8. (a) Specific heat (C_p) data of the EFCO compound over a temperature range of 1.8–305 K under zero magnetic field. Inset shows the zoomed view of the data showing an anomaly at ~ 3 K. (b) The low-temperature C_p data under $H = 0, 30,$ and 50 kOe magnetic fields and its fitting (black curve) using Eq. (1).

the following equation [63]:

$$C_p(T) = \beta T^3 + \beta_5 T^5 + \beta_7 T^7 + N \left(\frac{\Delta}{T} \right)^2 \left\{ \frac{\exp(\Delta/T)}{[1 + \exp(\Delta/T)]^2} \right\}. \quad (1)$$

Here, β , β_5 , and β_7 describe the phononic specific heat terms derived from the low-frequency expansion of the Debye function [64]; Δ ($\propto H$) is the splitting of the ground-state doublet of a magnetic ion (Er in the present case); and N/R is the number of free spins with R as the gas constant. It is evident from Fig. 8(b) that the low-temperature C_p data under zero magnetic field fit well with the above equation, and the derived parameters are $\beta = 1.45 \times 10^{-3} \text{ J mol}^{-1} \text{ K}^{-4}$, $\beta_5 = -2.16 \times 10^{-6} \text{ J mol}^{-1} \text{ K}^{-6}$, $\beta_7 = 1.17 \times 10^{-9} \text{ J mol}^{-1} \text{ K}^{-8}$, $N = 6.24 \text{ J mol}^{-1} \text{ K}^{-1}$, and $\Delta = 6.45 \text{ K}$. The values of derived phononic parameters (along with their signs) are comparable with the values reported for other similar compounds [12,65,66]. The derived $\Delta = 6.45 \text{ K}$ value is slightly higher than the reported value of 4.52 K for the ErFeO_3 compound as determined from the optical studies [37,67]; however, the value is quite close to the reported 5.6 K for the $\text{Er}_{0.5}\text{Dy}_{0.5}\text{FeO}_3$ compound [37]. Further, the C_p data under magnetic fields are also fitted with the above equation, and good agreement is observed [Fig. 8(b)]. The estimated value of Δ is 7.33 K (12.74 K) for 10 kOe (30 kOe), and it increases to 18.99 K for 50 kOe. A similar increase in the Δ value is reported in the literature for the $\text{Er}_{0.5}\text{Dy}_{0.5}\text{FeO}_3$ compound [37].

It is known that C_p data show a λ -shaped anomaly at the magnetic ordering temperature of the transition metal present in the sample. For instance, in Yb/Er/NdCrO_3 compounds, the λ -shaped anomaly at 120/133/220 K is attributed to the magnetic ordering of Cr spins owing to Cr-Cr superexchange interaction [12,68,69]. In the present EFCO compound, no λ -shaped anomaly corresponding to the ordering of Fe/Co spins is observed over the temperature range of 1.8–305 K because the magnetic ordering temperature of the compound is $> 310 \text{ K}$, as discussed earlier. On the other hand, at the magnetic ordering temperature of the rare earth, either a λ -shaped (like the transition metal) or Schottky anomaly is observed depending upon the strength of the exchange/molecular field of the transition metal experienced by the rare-earth spins. For instance, in the NdCoO_3 compound, authors reported a sharp λ -shaped anomaly in the C_p data corresponding to Nd ordering owing to Nd-Nd exchange interaction due to the nonmagnetic nature of Co, and the molecular field acting on the Nd ions was zero [70], while the finite exchange field on Nd spins in Nd(Fe/Ni/Cr)O_3 compounds due to magnetic ordering of Fe/Ni/Cr ions gives a Schottky anomaly-type feature in the C_p data of the corresponding compounds [65,69,70]. Thus, in the present EFCO compound, the molecular field of Fe/Co spins experienced by the Er spins may be higher than the Er-Er exchange interaction, leading to a Schottky anomaly instead of a λ -shaped anomaly in the C_p data of the compound. A similar Schottky anomaly, instead of a λ -shaped anomaly, at the magnetic ordering temperature of Sm spins was reported for the SmCrO_3 compound; however, the independent magnetic ordering of Sm due to Sm-Sm exchange

interaction was evident from the ND study [53,71], as is the case for the present EFCO compound.

5. Understanding of the NM

In the present EFCO compound, the dc magnetization data show anomalies at $T_{\text{SR}} \sim 100 \text{ K}$, $T_{\text{COMP}} (24 \text{ K})$, and $T_{\text{N}}^{\text{Er}} \sim 4 \text{ K}$ [Fig. 2(a)]. The microscopic understanding of these anomalies has been obtained from the ND study where the magnetic ordering of Fe/Co and Er spins into AFM $G_x(\Gamma_4)$, $G_z(\Gamma_2)$, and $A_y^{\text{Er}} C_z^{\text{Er}}(\Gamma_{57})$, respectively, are evident. It is known that, in $R\text{FeO}_3$ compounds, the AFM Fe spins cant due to the Dzyaloshinskii-Moriya interaction [27,28], and this small canting gives rise to a weak FM moment. The weak FM Fe/Co moments in the present compound lie along the z (F_z) and x (F_x) axes in Γ_4 and Γ_2 spin configurations and cannot be measured from the present powder ND study, though their signatures are evident from the dc magnetization studies [Figs. 2(a) and 2(b)]. It is also known that, in $R(\text{Fe/Cr})\text{O}_3$ compounds with magnetic rare-earth ions, at $T > T_{\text{N}}^{\text{R}}$, rare-earth ions polarize under the internal field (H_I) of the Cr/Fe sublattice either parallel or antiparallel to the net FM moment of Cr/Fe [29]. The polarization of Er moments in the present EFCO compound is evident from the monotonic increase in ac susceptibility at low temperatures [Fig. 2(c)] and the Schottky anomaly in the specific heat data [Fig. 8]. Thus, we have used the Cooke's model [72], which involves fitting of the dc magnetization data, to find the direction of the polarized Er moment M_{Er} with respect to the weak FM moment of Fe/Co ($M_{\text{Fe/Co}}$) in the EFCO compound. We used the same model in our recent reports on $\text{La}_{1-x}\text{Pr}_x\text{CrO}_3$ [11,14] and YbCrO_3 [12] compounds, and other researchers used it to explain the NM in $\text{NdCr}_{1-x}\text{Mn}_x\text{O}_3$ [43], $\text{ErFe}_{0.5}\text{Mn}_{0.5}\text{O}_3$ [73], and $\text{Y}_{1-x}\text{Pr}_x\text{CrO}_3$ [74] compounds. According to this model, the temperature dependence of the dc magnetization (M) under some applied magnetic field (H) around the T_{COMP} ($T < 50 \text{ K}$ for the present case) can be fitted to the following equation:

$$M = M_{\text{Fe/Co}} + C_{\text{Er}} \frac{(H + H_I)}{T + \theta}, \quad (2)$$

where $M_{\text{Fe/Co}}$ is the FM moment of the Fe/Co sublattice, C_{Er} is the Curie constant of the Er ion, θ is the Curie-Weiss constant, and H_I and H are internal and applied magnetic fields, respectively. The value of C_{Er} is $11.473 \text{ emu K Oe}^{-1} \text{ mol}^{-1}$, as determined from the effective paramagnetic moment of the Er ion ($\mu_{\text{eff}} = 9.58 \mu_{\text{B}}$). The M vs T curves for $H \leq 450 \text{ Oe}$ (the maximum field under which the compound shows NM) have been fitted with Eq. (2), and one of them is shown in Fig. 9, and the parameters $M_{\text{Fe/Co}}$ and H_I (see inset) are estimated. For the fitting under different applied magnetic fields, a constant value of $\theta \sim 10.7 \text{ K}$ was maintained. Using the derived $M_{\text{Fe/Co}}$ and $|H_I|$ values, T_{COMP} is calculated from Eq. (2) and found to match very well with the experimental values of T_{COMP} [see inset of Fig. 2(b)]. The fitted values of $M_{\text{Fe/Co}}$ and $|H_I|$ increase significantly with increasing H (inset of Fig. 9), as reported for other polycrystalline compounds viz. $\text{La}_{0.5}\text{Pr}_{0.5}\text{CrO}_3$ [11], YbCrO_3 [12], and $\text{NdCr}_{1-x}\text{Mn}_x\text{O}_3$ [43]. However, in the case of the ErFeO_3 single-crystal sample, Fita *et al.* [75] reported weakly increasing FM moment (M_{Fe}) as well as H_I as a function of H , which may be due to

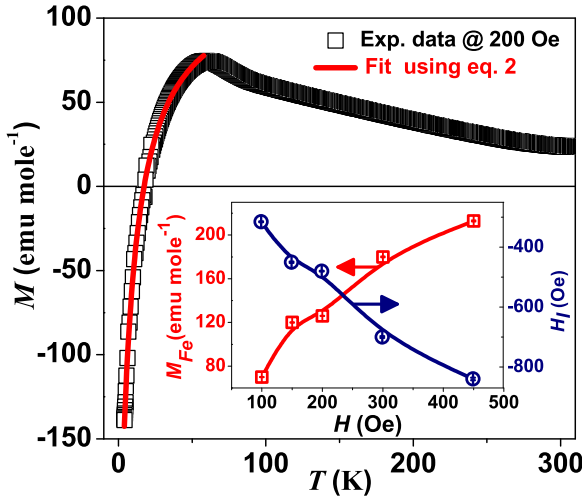


FIG. 9. Field-cooled-cooling M vs T curve (open square black symbols) measured under $H = 200$ Oe and its fitting using the Cooke's model (solid red line). Inset shows the variation of $M_{\text{Fe/Co}}$ and H_I with H . The solid lines in inset are guides to the eye.

the single-domain magnetic state of the sample, whereas for the present polycrystalline EFCO compound, the domain size grows under increasing H due to the multidomain structure of the sample. This leads to an increase in $M_{\text{Fe/Co}}$, which in turn increases H_I acting on the Er site. It should be noted that the derived H_I values are negative for all the fitted M vs T curves. The larger negative values of H_I in comparison with positive H make the effective field ($H + H_I$) negative, inferring the alignment of M_{Er} opposite to $M_{\text{Fe/Co}}$. At $T \leq T_{\text{COMP}}$, M_{Er} gets polarized more and more in the direction opposite to $M_{\text{Fe/Co}}$ and results in NM in the EFCO compound.

6. EB

The FC $M(H)$ hysteresis loops recorded at some of the selected temperatures under a cooling field (H_{COOL}) of 10 kOe are shown in Figs. S2(a)–S2(d) in the SM [46], while their enlarged views are shown in Figs. 10(a)–10(d). The FC $M(H)$ hysteresis loop shows a slight opening in the low magnetic-field region indicating the presence of a FM moment in the compound, and linear behavior at the high field region is attributed to the dominating AFM moment. We have estimated the hysteresis loop parameters viz. coercivity (H_C) and remanent magnetization (M_R) for all recorded loops using the expressions: $H_C = |H_{C1} - H_{C2}|/2$ and $M_R = |M_{R1} - M_{R2}|/2$, where H_{C1} (H_{C2}) and M_{R1} (M_{R2}) are the left (right) coercivity and up (down) remanent magnetization, respectively, corresponding to $M = 0$ and $H = 0$ during descending (ascending) branch of the hysteresis loop. Temperature variations of H_C and M_R are plotted in Fig. 11(a). It is found that, with decreasing temperature from 300 K, H_C increases and becomes maximum at $T \sim T_{\text{SR}}$. With further cooling, H_C decreases and shows a minimum value at $T \sim 33$ K [a temperature where ZFC and FC magnetization curves cross each other, Fig. 2(a)]. At $T < 33$ K, H_C increases gradually down to T_{COMP} [middle inset of Fig. 11(a)], and thereafter, a sharp rise in H_C in $T_{\text{COMP}} > T > 10$ K followed by a sharp decrease < 5 K [top left inset of Fig. 11(a)] are observed. The M_R follows a similar

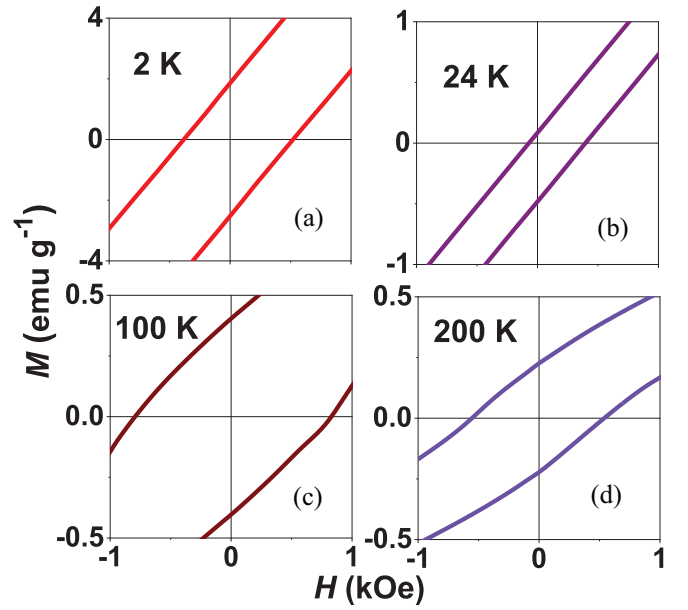


FIG. 10. Enlarged views of field-cooled $M(H)$ hysteresis loops at some of the temperatures under $H_{\text{COOL}} = 10$ kOe.

temperature dependence [Fig. 11(a); right scale] as that of H_C down to 10 K. At $T < 10$ K, a sharp rise in M_R is observed down to 2 K. The decrease in H_C below T_{SR} and T_{N}^{Er} is related to the SR and magnetic ordering of Fe/Co and Er spins, respectively. However, the increase in H_C below T_{COMP} may be attributed to the increasing polarization of the Er spins, as evident from the Schottky anomaly (Fig. 8) and the Cooke's model (Fig. 9), under the internal magnetic field of Fe/Co spins.

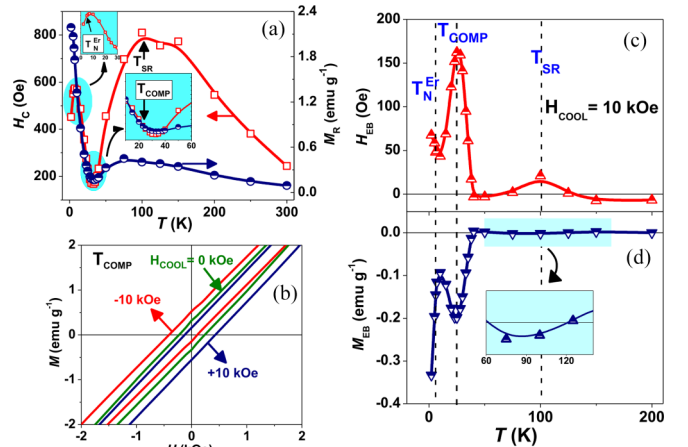


FIG. 11. Temperature dependencies of (a) H_C and M_R showing anomalies at T_{N}^{Er} , T_{COMP} , and T_{SR} . The middle inset in (a) shows the enlarged view of H_C and M_R curves in the vicinity of T_{COMP} , and the zoomed H_C behavior in the low-temperature region is shown in top left inset. (b) $M(H)$ loops recorded at T_{COMP} under $H_{\text{COOL}} = 0$ and ± 10 kOe. Here, the measurement range was ± 50 kOe; however, for clarity, magnetization data only up to ± 2 kOe are shown. Thermal variations of (c) H_{EB} and (d) M_{EB} , showing anomalies at T_{N}^{Er} , T_{COMP} , and T_{SR} , under $H_{\text{COOL}} = 10$ kOe. Inset in (d) shows the enlarged view of M_{EB} near T_{SR} .

Further, the $M(H)$ loops are found to be asymmetric along the horizontal (vertical) magnetic field (magnetization) axis (Fig. 10), indicating the presence of EB in the compound. Sometimes this loop shift arises due to the minor loop effect [76]. To exclude this effect, we have recorded the $M(H)$ loop at T_{COMP} (a temperature at which maximum EB is observed, discussed later) under $H_{\text{COOL}} = -10$ kOe in the N-type H -sweeping protocol: $(-50 \text{ kOe}) \rightarrow (0 \text{ kOe}) \rightarrow (+50 \text{ kOe}) \rightarrow (0 \text{ kOe}) \rightarrow (-50 \text{ kOe})$ [Fig. 11(b)], whereas $M(H)$ loops shown in Fig. 10 have been recorded in the P-type H -sweeping protocol: $(+50 \text{ kOe}) \rightarrow (0 \text{ kOe}) \rightarrow (-50 \text{ kOe}) \rightarrow (0 \text{ kOe}) \rightarrow (+50 \text{ kOe})$. The symmetric and opposite shifting of $M(H)$ loops recorded under $H_{\text{COOL}} = \pm 10$ kOe with respect to ZFC $M(H)$ loop [Fig. 11(b)] indicate that the observed loop shift or EB is not due to the minor loop effect.

The EB parameters H_{EB} and M_{EB} for the present compound are estimated using the following expressions: $H_{\text{EB}} = (H_{\text{C2}} + H_{\text{C1}})/2$ and $M_{\text{EB}} = (M_{\text{R1}} + M_{\text{R2}})/2$, where H_{EB} and M_{EB} represent the horizontal and vertical shifts, respectively, in the hysteresis loops. Figures 11(c) and 11(d) depict the thermal variations of H_{EB} and M_{EB} . Finite H_{EB} in the proximity of T_{N}^{Er} , T_{COMP} , and T_{SR} is evident from Fig. 11(c). At 200 K, H_{EB} is found to be slightly negative. With decreasing temperature, H_{EB} remains almost constant down to 120 K; thereafter, it shows a broad hump at T_{SR} with positive H_{EB} . With further decrease in temperature and < 50 K (a temperature where maximum positive magnetization is observed [Fig. 2(a)]), H_{EB} increases and interestingly becomes positively maximum at T_{COMP} . It may be recalled from Sec. III B 3 that T_{COMP} is the temperature where complete spin orientation takes place. Intriguing H_{EB} behavior at T_{COMP} and T_{SR} indicates a correlation between the EB and SR in the EFCO compound. We have also reported a correlation between EB and SR in DyFe_5Al_7 [50], and Padam *et al.* [77] have reported it in $\text{Co}(\text{Cr}_{1-x}\text{Fe}_x)_2\text{O}_4$. Further, at $T < T_{\text{COMP}}$, H_{EB} decreases followed by a small increase at $T < T_{\text{N}}^{\text{Er}}$. The maximum H_{EB} at $T = T_{\text{COMP}}$ in the present NM EFCO compound is consistent with RFeO_3 ($R = \text{Nd}$ and Er) compounds [22] showing NM. The positive H_{EB} at $T < T_{\text{COMP}}$ is also in agreement with RFeO_3 ($R = \text{Nd}$ and Er) [22], $\text{La}_{0.5}\text{Pr}_{0.5}\text{CrO}_3$ [11], YbCrO_3 [12], SmFeO_3 [30], $\text{RFe}_{0.5}\text{Cr}_{0.5}\text{O}_3$ ($R = \text{Lu}$ and Nd) [31,32], and $\text{NdCr}_{1-x}\text{Mn}_x\text{O}_3$ [43] compounds. However, the positive H_{EB} in the present EFCO compound even at $T > T_{\text{COMP}}$ is quite exotic in comparison with the negative H_{EB} reported in all the above-mentioned literature compounds. It is also worthy to note that the maximum H_{EB} at $T = T_{\text{COMP}}$ in the present EFCO compound is different in comparison with the zero value reported for compounds shown in Refs. [11,12,30–32,43]. Thus, based on the reported EB behavior in NM compounds and their comparison with the present one, an unusual H_{EB} in the present EFCO compound is evident. The M_{EB} varies like H_{EB} , albeit with the opposite sign and interestingly showing anomalies at T_{N}^{Er} , T_{COMP} , and T_{SR} [Fig. 11(d)].

The observed H_{EB} behavior in the present EFCO compound can be explained qualitatively with the model given in the literature [78]. According to this model, H_{EB} is represented as $H_{\text{EB}} = J_{\text{INT}}/|M_{\text{Net}}| \cos \theta$, where J_{INT} is the exchange-coupling constant between two AFM coupled sublattices and is negative [26], M_{Net} is the net magnetization, and θ is the angle between M_{Net} and H . This model is reminiscent of that

given by Meiklejohn and Bean [7] to explain H_{EB} behavior in FM/AFM interfacial systems. At $T \sim T_{\text{COMP}}$, M_{Net} is very small [Fig. 2(a)]; therefore, as per the above model, H_{EB} diverges at T_{COMP} [Fig. 11(c)] for the EFCO compound. A similar explanation is given in the literature to elucidate the maximum H_{EB} at T_{COMP} of 150 and 45 K in single crystals of GdCrO_3 [13] and ErFeO_3 [21] compounds, respectively. Further, for the present compound, this model explains the H_{EB} behavior in $T_{\text{N}}^{\text{Er}} < T < T_{\text{COMP}}$ very well because, in this temperature range, net magnetization $|M_{\text{Net}}|$ is increasing with decreasing temperature below T_{COMP} [Fig. 2(a)], consequently H_{EB} decreases as per the above model. The small rise in H_{EB} below T_{N}^{Er} is attributed to the magnetic ordering of Er spins, as evident from our ND study. The above model also explains the H_{EB} sign below T_{COMP} . At $T < T_{\text{COMP}}$, $|M_{\text{Net}}|$ orients opposite to H , making $\theta = \pi$ or $\cos \theta = -1$ (negative) and $J_{\text{INT}} < 0$. This gives H_{EB} positive which is consistent with the literature of related compounds [11,12,14,18,30–32]. Interestingly, the present EFCO compound shows positive H_{EB} even at $T > T_{\text{COMP}}$, indicating the unusual EB in comparison with the usual EB with negative H_{EB} at $T > T_{\text{COMP}}$ reported for YbCrO_3 [12], ErFeO_3 [21], SmFeO_3 [30], and other related compounds [31,32]. This shows that the positive H_{EB} at $T > T_{\text{COMP}}$ is generally not common in all NM compounds; however, it has been reported in a few NM compounds, such as $\text{Nd}_{0.75}\text{Ho}_{0.25}\text{Al}_2$ [19] and GdCo_2/Co multilayers [79]. It is also interesting to note that a positive H_{EB} at $T > T_{\text{COMP}}$ was realized in the ErFeO_3 single crystal [21] when using the field-heating mode (as opposite to field cooling), as a result of which H was directed oppositely to the canted FM moment M_{Fe} at the beginning of the $M(H)$ loop. It should be noted that, in these systems, magnetic moments do not exhibit the SR in the measured EB range. This indicates that the SR of Fe/Co spins in the present EFCO compound leads to the complex exchange coupling between Er and Fe/Co spins which may be responsible for the observed unusual EB effect at $T > T_{\text{COMP}}$.

For further understanding of the EB in the present EFCO compound, $M(H)$ hysteresis loops, under various H_{COOL} , have been recorded at T_{COMP} (24 K), a temperature at which maximum EB is observed. Some of them (enlarged view) are shown in Fig. 12(a), and the variations of H_{EB} and $-M_{\text{EB}}$ with H_{COOL} are plotted in Fig. 12(b). It is evident that both H_{EB} and $|M_{\text{EB}}|$ first sharply increase with increasing H_{COOL} , become maximum at $H_{\text{COOL}} \sim 5$ kOe, and remain constant up to $H_{\text{COOL}} = 20$ kOe, followed by a gradual decrease with further increase in H_{COOL} up to 70 kOe (maximum H_{COOL} used in this paper). The H_{EB} and $|M_{\text{EB}}|$ behaviors, i.e., first increase with H_{COOL} and then constant, are usual and reported in many single-phase compounds such as YbCrO_3 [12], DyFe_5Al_7 [50], $\text{Dy}_{0.33}\text{Nd}_{0.67}\text{CrO}_3$ [80], and TbMn_2Si_2 [81]. However, a decrease in H_{EB} and $|M_{\text{EB}}|$ at higher H_{COOL} is rarely observed and is reported in only a few compounds such as $\text{La}_{0.5}\text{Pr}_{0.5}\text{CrO}_3$ [11], $\text{LuFe}_{0.5}\text{Cr}_{0.5}\text{O}_3$ [31], $\text{YFe}_{0.5}\text{Cr}_{0.5}\text{O}_3$ [82], and $\text{Dy}_{0.2}\text{Nd}_{0.8}\text{CrO}_3$ [83]. Sharma *et al.* [82] explained the decreasing $H_{\text{EB}}/|M_{\text{EB}}|$ under higher H_{COOL} in the $\text{YFe}_{0.5}\text{Cr}_{0.5}\text{O}_3$ compound by considering the competition between effective Zeeman and interfacial exchange energies between FM and AFM regions. At higher H_{COOL} , more and more FM spins align in the direction of H_{COOL} , causing $H_{\text{EB}}/|M_{\text{EB}}|$ to decrease. In $\text{LuFe}_{0.5}\text{Cr}_{0.5}\text{O}_3$ [31], the decrease

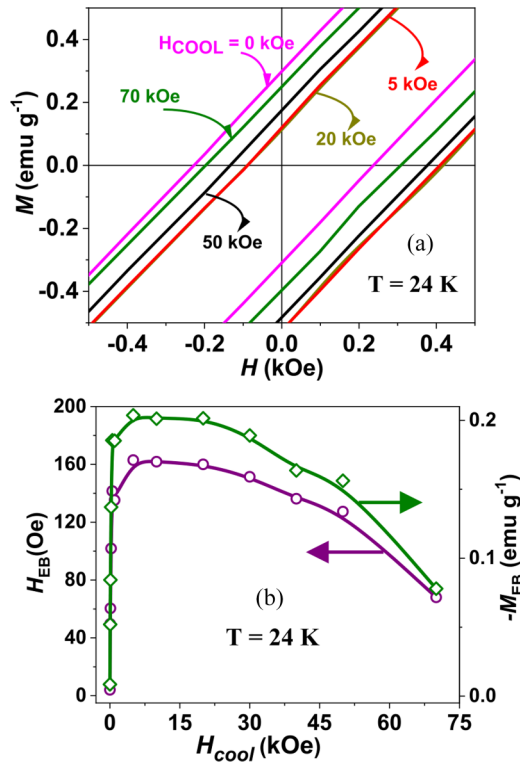


FIG. 12. (a) Zoomed view of the $M(H)$ loops recorded under various H_{COOL} at $T_{\text{COMP}} = 24$ K. (b) Variations of H_{EB} (left scale) and $-M_{\text{EB}}$ (right scale) with H_{COOL} at T_{COMP} .

of $H_{\text{EB}}/|M_{\text{EB}}|$ was explained by considering the competition of various Dzyaloshinskii-Moriya interactions between Fe^{3+} and Cr^{3+} spins. The competition between Pr^{3+} and Cr^{3+} moments was responsible for the decrease in $H_{\text{EB}}/|M_{\text{EB}}|$ at higher H_{COOL} in $\text{La}_{0.5}\text{Pr}_{0.5}\text{CrO}_3$ [11]. These reported studies suggest the role of the exchange coupling between the two competing magnetic sublattices, which for the present EFCO compound are Fe/Co and Er, in explaining the decrease in $H_{\text{EB}}/|M_{\text{EB}}|$ at higher H_{COOL} . Recently, Zhang *et al.* [84] studied the single crystal of ErFeO_3 , a compound like the present EFCO, in a static and pulsed magnetic field using magnetization study. They showed that magnetic interactions between Er and Fe moments get weaker at higher magnetic fields. This weakens the exchange coupling between two sublattices, causing $H_{\text{EB}}/|M_{\text{EB}}|$ to decrease at higher H_{COOL} in the present EFCO compound.

IV. DISCUSSION ON ER ORDERING

Now we discuss the unusual Er ordering into Γ_{57} IR in the present EFCO compound. It is known from the literature that the IRs of the R and Fe spins in a given $R\text{FeO}_3$ compound may or may not be the same. For instance, the magnetic ordering of Fe spins into $\Gamma_2(G_z)$ is compatible with the rare-earth ($R = \text{Nd}, \text{Sm}, \text{and Ho}$) ordering into the same $\Gamma_2(F_x, C_y)$ IR [26,57,58]. Similar compatible IRs of rare-earth and Fe spins are reported for doped orthoferrites, $\text{Nd}_{0.5}\text{Dy}_{0.5}\text{FeO}_3$ [35], $\text{Er}_{0.5}\text{Dy}_{0.5}\text{FeO}_3$ [37], and $R\text{Fe}_{0.5}\text{Cr}_{0.5}\text{O}_3$ ($R = \text{Tb}, \text{Ho}, \text{and Er}$) [38]. However, for ErFeO_3 [56] and $\text{HoFe}_{0.5}\text{Co}_{0.5}\text{O}_3$ [42] compounds, Er and Ho orderings into $\Gamma_1(C_z)$ and $\Gamma_2(F_x, C_y)$

IRs are not compatible with the $\Gamma_2(G_z)$ and $\Gamma_{14}(G_y, G_x)$ IRs of Fe and Fe/Co spins, respectively. Here, it must be noted that, in all above-mentioned compounds, rare-earth orders either into Γ_1 or Γ_2 , which give intensity to $\{(100)(010)\}$ or (100) Bragg peaks, respectively. These Bragg peaks are not found in the present ND data [Fig. 4(a)]; thus, the possibility of Er ordering into Γ_1 or Γ_2 spin configurations is excluded. Further, the ND studies on SmCrO_3 [53] and DyFeO_3 [55] compounds revealed the Sm and Dy ordering (at low temperatures) into Γ_7 and Γ_{57} spin configurations, respectively. In the DyFeO_3 compound, it is reported that $\Gamma_5(A_y)$ of Dy accounts for the intensity of the (001) Bragg peak, while the enhanced intensity of (011) is accounted by $\Gamma_7(G_z)$, which is consistent with our ND results (Fig. 4). Further, Biswas *et al.* [55] and Citter *et al.* [85] recently showed the splitting of the (001) Bragg peak positioned at $Q = 0.84 \text{ \AA}^{-1}$ into a doublet using high-resolution ND data on the DyFeO_3 compound. At ~ 2 K, the ND was fitted with a nonzero propagation vector ($k_z = 0.017$ [55] and 0.028 [85]), leading to the incommensurate ordering of the Dy sublattice in the DyFeO_3 compound. Our inference of Er ordering into the Γ_{57} spin configuration in the present EFCO compound from ND results matches well with reported results on the DyFeO_3 compound. However, splitting of the (001) Bragg peak could not be confirmed from our present ND data [Fig. 4(a)], which may be due to the limited resolution of our ND instrument. Further, according to Yamaguchi *et al.* [86], the magnetic ordering into the Γ_5 - Γ_8 spin configuration leads to the magnetoelectric effect in the compound, which is extensively studied in the DyFeO_3 compound [24,87]. Thus, based on the literature reports, further studies in the EFCO compound would be worthy of investigation.

V. SUMMARY AND CONCLUSIONS

We have studied the structural and magnetic properties of the $\text{ErFe}_{0.5}\text{Co}_{0.5}\text{O}_3$ (EFCO) compound using x-ray diffraction, EDX, dc magnetization, ac susceptibility, specific heat, neutron depolarization, and ND experimental techniques. The dc magnetization study reveals the NM phenomenon in the compound with the compensation temperature (T_{COMP}) of 24 K. The Rietveld refinement of ND patterns over 1.5–300 K infers the onset of SR transition at 100 K (T_{SR}) in the compound, leading to the different magnetic structures over different temperature ranges. In the 300–100 K range, the magnetic structure of the compound is $\Gamma_4(G_x)$, which changes to $\Gamma_2(G_z)$ at T_{COMP} after going through the intermediate Γ_{24} structure in the temperature range of $T_{\text{COMP}} < T \leq T_{\text{SR}}$. The marked anomalies are observed in ac susceptibility data at T_{SR} and T_{COMP} . Interestingly, < 4 K (T_{N}^{Er}), Er shows magnetic ordering into an unusual $\Gamma_{57}(A_y, G_z^{\text{Er}})$ spin configuration. However, at $T > T_{\text{N}}^{\text{Er}}$, the Er moment (M_{Er}) is polarized under the internal field of ordered Fe/Co moments. The polarized nature of the Er moment is evident from the Schottky anomaly observed in the specific heat data and monotonic increase in the ac susceptibility below T_{COMP} . The observed NM in the present compound is explained within the framework of the Cooke's model, where M_{Er} competes with the weak FM component ($M_{\text{Fe/Co}}$) of canted AFM Fe/Co moments. The negative internal magnetic field, derived from the Cooke's model, aligns M_{Er} in an opposite direction to $M_{\text{Fe/Co}}$ as well as

to the applied magnetic field below T_{COMP} , thus bringing the compound to the NM state.

Further, the FC hysteresis loops reveal that the compound exhibits anomalous behaviors of coercivity and remanent magnetization showing marked anomalies at T_{SR} , T_{COMP} , and T_{N}^{Er} . Interestingly, the compound shows unusual positive H_{EB} (EB field) at $T > T_{\text{COMP}}$ which could be attributed to the complex spin arrangement (SR) of Fe/Co spins. A correlation between EB and SR is also evident from the maximum positive H_{EB} and broad hump in H_{EB} at T_{COMP} and T_{SR} , respectively. Moreover, the EB behavior involving positive H_{EB} at $T < T_{\text{COMP}}$ along with its maximum value at T_{COMP} is explained within the framework of the model reminiscent of the model of Meiklejohn and Bean [7]. The unusual EB involving a nonmonotonic variation of H_{EB} with cooling

magnetic field is also found in the compound. Such unusual temperature- and magnetic-field-dependent magnetic properties make the EFCO compound a promising candidate for application in magnetic memories, thermomagnetic switches, and other spintronic devices.

ACKNOWLEDGMENTS

D.G. acknowledges P. S. R. Krishna, A. B. Shinde, and A. Das for their help in ND (PD-II) measurements. D.G. also acknowledges P. D. Babu for the specific heat measurements. S.M.Y. acknowledges the financial assistance from Science and Engineering Research Board (SERB), Department of Science and Technology, Government of India under the J. C. Bose fellowship program (Grant No. JCB/2023/000014).

-
- [1] A. Kumar and S. M. Yusuf, The phenomenon of negative magnetization and its implications, *Phys. Rep.* **556**, 1 (2015).
- [2] S. M. Yusuf, A. Kumar, and J. V. Yakhmi, Temperature- and magnetic-field-controlled magnetic pole reversal in a molecular magnetic compound, *Appl. Phys. Lett.* **95**, 182506 (2009).
- [3] P. K. Manna and S. M. Yusuf, Two interface effects: Exchange bias and magnetic proximity, *Phys. Rep.* **535**, 61 (2014).
- [4] J. Nogués, J. Sort, V. Langlais, V. Skumryev, S. Suriñach, J. S. Muñoz, and M. D. Baró, Exchange bias in nanostructures, *Phys. Rep.* **422**, 65 (2005).
- [5] J. C. S. Kools, Exchange-biased spin-valves for magnetic storage, *IEEE Trans. Magn.* **32**, 3165 (1996).
- [6] S. Ivanova, A. Senyshyn, E. Zhecheva, K. Tenchev, R. Stoyanova, and H. Fuess, Robust isothermal electric control of exchange bias at room temperature, *J. Solid State Chem.* **183**, 940 (2010).
- [7] W. H. Meiklejohn and C. P. Bean, New magnetic anisotropy, *Phys. Rev.* **102**, 1413 (1956).
- [8] A. Hoffmann, M. Grimsditch, J. E. Pearson, J. Nogués, W. A. A. Macedo, and I. K. Schuller, Tailoring the exchange bias via shape anisotropy in ferromagnetic/antiferromagnetic exchange-coupled systems, *Phys. Rev. B* **67**, 220406(R) (2003).
- [9] X. Ke, M. S. Rzechowski, L. J. Belenky, and C. B. Eom, Positive exchange bias in ferromagnetic $\text{La}_{0.67}\text{Sr}_{0.33}\text{MnO}_3/\text{SrRuO}_3$ bilayers, *Appl. Phys. Lett.* **84**, 5458 (2004).
- [10] E. Maniv, R. A. Murphy, S. C. Haley, S. Doyle, C. John, A. Maniv, S. K. Ramakrishna, Y. Tang, P. Ercius, R. Ramesh *et al.*, Exchange bias due to coupling between coexisting antiferromagnetic and spin-glass orders, *Nat. Phys.* **17**, 525 (2021).
- [11] Deepak, A. Kumar, and S. M. Yusuf, Correlation of exchange-bias effect with negative magnetization in perovskite compound, $\text{La}_{0.5}\text{Pr}_{0.5}\text{CrO}_3$, *J. Appl. Phys.* **127**, 213903 (2020).
- [12] Deepak, A. Kumar, and S. M. Yusuf, Intertwined magnetization and exchange bias reversals across compensation temperature in YbCrO_3 compound, *Phys. Rev. Mater.* **5**, 124402 (2021).
- [13] I. Fita, R. Puzniak, A. Wisniewski, and V. Markovich, Spin switching and unusual exchange bias in the single crystalline GdCrO_3 compensated ferrimagnet, *Phys. Rev. B* **100**, 144426 (2019).
- [14] Deepak, A. Kumar, A. K. Bera, and S. M. Yusuf, Correlated negative magnetization, exchange bias, and electrical properties in $\text{La}_{1-x}\text{Pr}_x\text{CrO}_3$, *Phys. Rev. Mater.* **6**, 074405 (2022).
- [15] J. Barman, P. D. Babu, and S. Ravi, Exchange bias and magnetization reversal in $\text{Ni}(\text{Cr}_{1-x}\text{Fe}_x)_2\text{O}_4$ ($x = 0-0.20$), *J. Magn. Magn. Mater.* **418**, 300 (2016).
- [16] J. Barman and S. Ravi, Sign reversal of magnetization and exchange bias in $\text{Ni}(\text{Cr}_{1-x}\text{Al}_x)_2\text{O}_4$ ($x = 0-0.50$), *J. Magn. Magn. Mater.* **426**, 82 (2017).
- [17] F. Hong, Z. Cheng, J. Wang, X. Wang, and S. Dou, Positive and negative exchange bias effects in the simple perovskite manganite NdMnO_3 , *Appl. Phys. Lett.* **101**, 102411 (2012).
- [18] B. B. Dash and S. Ravi, Magnetization reversal and tunable exchange bias in $\text{GdCr}_{1-x}\text{Mn}_x\text{O}_3$ ($x = 0-0.50$), *J. Magn. Magn. Mater.* **429**, 281 (2017).
- [19] P. D. Kulkarni, A. Thamizhavel, V. C. Rakhecha, A. K. Nigam, P. L. Paulose, S. Ramakrishnan, and A. K. Grover, Magnetic compensation phenomenon and the sign reversal in the exchange bias field in a single crystal of $\text{Nd}_{0.75}\text{Ho}_{0.25}\text{Al}_2$, *Europhys. Lett.* **86**, 47003 (2009).
- [20] S. Venkatesh, U. Vaidya, V. Rakhecha, S. Ramakrishnan, and A. Grover, Magnetic response in the vicinity of magnetic compensation: A case study in spin ferromagnetic $\text{Sm}_{1-x}\text{Gd}_x\text{Al}_2$ intermetallic alloys, *J. Phys.: Condens. Matter* **22**, 496002 (2010).
- [21] I. Fita, A. Wisniewski, R. Puzniak, V. Markovich, and G. Gorodetsky, Exchange-bias reversal in magnetically compensated ErFeO_3 single crystal, *Phys. Rev. B* **93**, 184432 (2016).
- [22] I. Fita, A. Wisniewski, R. Puzniak, E. E. Zubov, V. Markovich, and G. Gorodetsky, Common exchange-biased spin switching mechanism in orthoferrites, *Phys. Rev. B* **98**, 094421 (2018).
- [23] I. L. Prejbeanu, M. Kerekes, R. C. Sousa, H. Sibuet, O. Redon, B. Dieny, and J. P. Nozières, Thermally assisted MRAM, *J. Phys.: Condens. Matter* **19**, 165218 (2007).
- [24] Y. Tokunaga, S. Iguchi, T. Arima, and Y. Tokura, Magnetic-field-induced ferroelectric state in DyFeO_3 , *Phys. Rev. Lett.* **101**, 097205 (2008).
- [25] C.-Y. Kuo, Y. Drees, M. T. Fernández-Díaz, L. Zhao, L. Vasylechko, D. Sheptyakov, A. M. T. Bell, T. W. Pi, H.-J. Lin, M.-K. Wu *et al.*, $k = 0$ magnetic structure and absence of ferroelectricity in SmFeO_3 , *Phys. Rev. Lett.* **113**, 217203 (2014).
- [26] R. L. White, Review of recent work on the magnetic and spectroscopic properties of the rare-earth orthoferrites, *J. Appl. Phys.* **40**, 1061 (1969).

- [27] I. Dzyaloshinsky, A thermodynamic theory of weak ferromagnetism of antiferromagnetics, *J. Phys. Chem. Solids* **4**, 241 (1958).
- [28] T. Moriya, New mechanism of anisotropic superexchange interaction, *Phys. Rev. Lett.* **4**, 228 (1960).
- [29] T. Yamaguchi, Theory of spin reorientation in rare-earth orthochromites and orthoferrites, *J. Phys. Chem. Solids* **35**, 479 (1974).
- [30] C. De, A. K. Nayak, M. Nicklas, and A. Sundaresan, Magnetic compensation-induced sign reversal of exchange bias in a multi-glass perovskite SmFeO_3 , *Appl. Phys. Lett.* **111**, 182403 (2017).
- [31] I. Fita, V. Markovich, A. S. Moskvin, A. Wisniewski, R. Puzniak, P. Iwanowski, C. Martin, A. Maignan, R. E. Carbonio, M. U. Gutowska *et al.*, Reversed exchange-bias effect associated with magnetization reversal in the weak ferrimagnet $\text{LuFe}_{0.5}\text{Cr}_{0.5}\text{O}_3$, *Phys. Rev. B* **97**, 104416 (2018).
- [32] M. P. Sharannia, S. De, R. Singh, A. Das, R. Nirmala, and P. N. Santhosh, Observation of magnetization and exchange bias reversals in $\text{NdFe}_{0.5}\text{Cr}_{0.5}\text{O}_3$, *J. Magn. Magn. Mater.* **430**, 109 (2017).
- [33] B. Dalal, B. Sarkar, S. Rayaprol, M. Das, V. Siruguri, P. Mandal, and S. K. De, Unveiling ferrimagnetic ground state, anomalous behavior of the exchange-bias field around spin reorientation, and magnetoelectric coupling in $\text{YbCr}_{1-x}\text{Fe}_x\text{O}_3$ ($0.1 \leq x \leq 0.6$), *Phys. Rev. B* **101**, 144418 (2020).
- [34] A. Singh, A. Jain, A. Ray, P. Balasubramanian, R. Yadav, V. Nassif, S. Husain, S. M. Yusuf, T. Maitra, and V. K. Malik, Spin reorientation in $\text{NdFe}_{0.5}\text{Mn}_{0.5}\text{O}_3$: Neutron scattering and *ab initio* study, *Phys. Rev. B* **96**, 144420 (2017).
- [35] A. Singh, S. Rajput, P. Balasubramanian, M. Anas, F. Damay, C. M. N. Kumar, G. Eguchi, A. Jain, S. M. Yusuf, T. Maitra *et al.*, Successive spin reorientations and rare earth ordering in $\text{Nd}_{0.5}\text{Dy}_{0.5}\text{FeO}_3$: Experimental and *ab initio* investigations, *Phys. Rev. B* **102**, 144432 (2020).
- [36] H. Wu, S. Cao, M. Liu, Y. Cao, B. Kang, J. Zhang, and W. Ren, Twofold spin reorientation and field-induced incomplete phase transition in single-crystal $\text{Dy}_{0.5}\text{Pr}_{0.5}\text{FeO}_3$, *Phys. Rev. B* **90**, 144415 (2014).
- [37] S. Rajput, P. Balasubramanian, A. Singh, F. Damay, C. M. N. Kumar, W. Tabis, T. Maitra, and V. K. Malik, Coexisting magnetic structures and spin reorientation in $\text{Er}_{0.5}\text{Dy}_{0.5}\text{FeO}_3$: Bulk magnetization, neutron scattering, specific heat, and density functional theory studies, *Phys. Rev. B* **105**, 214436 (2022).
- [38] J. P. Bolletta, F. Pomiro, R. D. Sánchez, V. Pomjakushin, G. Aurelio, A. Maignan, C. Martin, and R. E. Carbonio, Spin reorientation and metamagnetic transitions in $R\text{Fe}_{0.5}\text{Cr}_{0.5}\text{O}_3$ perovskites ($R = \text{Tb}, \text{Dy}, \text{Ho}, \text{Er}$), *Phys. Rev. B* **98**, 134417 (2018).
- [39] A. Muñoz, M. Martínez-Lope, J. Alonso, and M. Fernández-Díaz, Magnetic structures of HoCoO_3 and TbCoO_3 , *Eur. J. Inorg. Chem.* **2012**, 5825 (2012).
- [40] K. Knížek, Z. Jiráček, P. Novák, and C. de la Cruz, Non-collinear magnetic structures of TbCoO_3 and DyCoO_3 , *Solid State Sci.* **28**, 26 (2014).
- [41] J. Padilla-Pantoja, J. L. García-Muñoz, J. A. Alonso, and M. T. Fernández-Díaz, Structural effects of the spin-state crossover at high temperature in the distorted ErCoO_3 cobaltite, *J. Phys.: Conf. Ser.* **663**, 012005 (2015).
- [42] J. Lohr, F. Pomiro, V. Pomjakushin, J. Alonso, R. Carbonio, and R. Sánchez, Multiferroic properties of $R\text{Fe}_{0.5}\text{Co}_{0.5}\text{O}_3$ with $R = \text{Tm}, \text{Er}, \text{Ho}, \text{Dy}$, and Tb , *Phys. Rev. B* **98**, 134405 (2018).
- [43] T. Bora and S. Ravi, Bipolar switching of magnetization and tunable exchange bias in $\text{NdCr}_{1-x}\text{Mn}_x\text{O}_3$ ($x = 0.0-0.30$), *J. Appl. Phys.* **116**, 063901 (2014).
- [44] H. Rietveld, A profile refinement method for nuclear and magnetic structures, *J. Appl. Cryst.* **2**, 65 (1969).
- [45] J. Rodríguez-Carvajal, Recent advances in magnetic structure determination by neutron powder diffraction, *Physica B* **192**, 55 (1993).
- [46] See Supplemental Material at <http://link.aps.org/supplemental/10.1103/PhysRevB.110.104401> for details on the crystallographic parameters of the EFCO compound at 300 and 1.5 K derived from the Rietveld refinement of the ND data, EDX spectrum, and FC hysteresis loops at some selected temperatures.
- [47] O. Halpern and T. Holstein, On the passage of neutrons through ferromagnets, *Phys. Rev.* **59**, 960 (1941).
- [48] S. M. Yusuf, M. Sahana, K. Dörr, U. K. Röbber, and K. H. Müller, Effect of Ga doping for Mn on the magnetic properties of $\text{La}_{0.67}\text{Ca}_{0.33}\text{MnO}_3$, *Phys. Rev. B* **66**, 064414 (2002).
- [49] I. Dhiman, A. Das, R. Mittal, Y. Su, A. Kumar, and A. Radulescu, Diffuse neutron scattering study of magnetic correlations in half-doped $\text{La}_{0.5}\text{Ca}_{0.5-x}\text{Sr}_x\text{MnO}_3$ manganites ($x = 0.1, 0.3$, and 0.4), *Phys. Rev. B* **81**, 104423 (2010).
- [50] Deepak, A. Kumar, S. M. Yusuf, and E. V. Sampathkumaran, Insight into the negative magnetization and anomalous exchange-bias in DyFe_5Al_7 through neutron depolarization and neutron diffraction studies, *J. Phys.: Condens. Matter* **35**, 065802 (2023).
- [51] M. Ghanathe, A. Kumar, and S. M. Yusuf, Microscopic and mesoscopic understanding of magnetization compensation phenomenon in ferrimagnetic $\text{Li}_{0.5}\text{FeCr}_{1.5}\text{O}_4$ spinel, *J. Appl. Phys.* **125**, 093903 (2019).
- [52] A. Kumar, S. M. Yusuf, and C. Ritter, Nd-ordering-driven Mn spin reorientation and magnetization reversal in the magnetototally coupled compound NdMnO_3 , *Phys. Rev. B* **96**, 014427 (2017).
- [53] T. Sau, P. Yadav, S. Sharma, R. Raghunathan, P. Manuel, V. Petricek, U. P. Deshpande, and N. P. Lalla, High-resolution time of flight neutron diffraction and magnetization studies of spin reorientation and polar transitions in SmCrO_3 , *Phys. Rev. B* **103**, 144418 (2021).
- [54] E. Bertaut, Representation analysis of magnetic structures, *Acta Cryst. A* **24**, 217 (1968).
- [55] B. Biswas, V. F. Michel, Ø. S. Fjellvåg, G. Bimashofer, M. Döbeli, M. Jambor, L. Keller, E. Müller, V. Ukleev, E. V. Pomjakushina *et al.*, Role of Dy on the magnetic properties of orthorhombic DyFeO_3 , *Phys. Rev. Mater.* **6**, 074401 (2022).
- [56] G. Deng, P. Guo, W. Ren, S. Cao, H. E. Maynard-Casely, M. Avdeev, and G. J. McIntyre, The magnetic structures and transitions of a potential multiferroic orthoferrite ErFeO_3 , *J. Appl. Phys.* **117**, 164105 (2015).
- [57] W. Sławiński, R. Przeniosło, I. Sosnowska, and E. Suard, Spin reorientation and structural changes in NdFeO_3 , *J. Phys.: Condens. Matter* **17**, 4605 (2005).
- [58] P. Prakash, V. Sathe, C. L. Prajapat, A. K. Nigam, P. S. R. Krishna, and A. Das, Spin phonon coupling in Mn doped HoFeO_3 compounds exhibiting spin reorientation behaviour, *J. Phys.: Condens. Matter* **32**, 095801 (2019).

- [59] R. W. Grant and S. Geller, Mechanism of spin reorientation in ErFeO_3 , *Solid State Commun.* **7**, 1291 (1969).
- [60] Z. Zhou, L. Guo, H. Yang, Q. Liu, and F. Ye, Hydrothermal synthesis and magnetic properties of multiferroic rare-earth orthoferrites, *J. Alloys Compd.* **583**, 21 (2014).
- [61] S. Katba, S. Jethva, M. Vagadia, A. Ravalia, and D. G. Kuberkar, Effect of La-substitution on magnetic properties of ErFeO_3 orthoferrites, *J. Magn. Magn. Mater.* **514**, 167170 (2020).
- [62] R. K. Zheng, A. N. Tang, Y. Yang, W. Wang, G. Li, X. G. Li, and H. C. Ku, Transport, magnetic, specific heat, internal friction, and shear modulus in the charge ordered $\text{La}_{0.25}\text{Ca}_{0.75}\text{MnO}_3$ manganite, *J. Appl. Phys.* **94**, 514 (2003).
- [63] X. M. Wang, Z. Y. Zhao, C. Fan, X. G. Liu, Q. J. Li, F. B. Zhang, L. M. Chen, X. Zhao, and X. F. Sun, Low-temperature heat transport, specific heat, and magnetic properties of the hexagonal TmMnO_3 single crystals, *Phys. Rev. B* **86**, 174413 (2012).
- [64] A. Tari, *The Specific Heat of Matter at Low Temperatures* (World Scientific, Singapore, 2003).
- [65] S. A. Mir, M. Ikram, and K. Asokan, Investigating spin reversal and other anomalies in magnetic, transport and specific heat measurements of NdFeO_3 and $\text{NdFe}_{0.5}\text{Ni}_{0.5}\text{O}_3$ orthoperovskites, *RSC Adv.* **5**, 85082 (2015).
- [66] Q. J. Li, Z. Y. Zhao, H. D. Zhou, W. P. Ke, X. M. Wang, C. Fan, X. G. Liu, L. M. Chen, X. Zhao, and X. F. Sun, Paramagnetic ground state with field-induced partial order in $\text{Nd}_3\text{Ga}_5\text{SiO}_{14}$ probed by low-temperature heat transport, *Phys. Rev. B* **85**, 174438 (2012).
- [67] D. L. Wood, L. M. Holmes, and J. P. Remeika, Exchange fields and optical Zeeman effect in ErFeO_3 , *Phys. Rev.* **185**, 689 (1969).
- [68] Y. Su, J. Zhang, L. Li, B. Li, Y. Zhou, D. Deng, Z. Chen, and S. Cao, Temperature dependence of magnetic properties and change of specific heat in perovskite ErCrO_3 chromites, *Appl. Phys. A* **100**, 73 (2010).
- [69] F. Bartolome, J. Bartolomé, M. Castro, and J. Melero, Specific heat and magnetic interactions in NdCrO_3 , *Phys. Rev. B* **62**, 1058 (2000).
- [70] F. Bartolomé, M. D. Kuz'min, J. Bartolomé, J. Blasco, J. García, and F. Sapiña, Low-temperature specific heat of NdMO_3 ($M = \text{Co, Fe, Cr, Ni}$): Magnetic ordering of Nd, *Solid State Commun.* **91**, 177 (1994).
- [71] P. Gupta and P. Poddar, Study of magnetic and thermal properties of SmCrO_3 polycrystallites, *RSC Adv.* **6**, 82014 (2016).
- [72] A. H. Cooke, D. M. Martin, and M. R. Wells, Magnetic interactions in gadolinium orthochromite, GdCrO_3 , *J. Phys. C Solid State Phys.* **7**, 3133 (1974).
- [73] K. Chandran, P. N. Lekshmi, and P. N. Santhosh, High temperature spin reorientation, magnetization reversal and magnetocaloric effect in 50% Mn substituted polycrystalline ErFeO_3 , *J. Solid State Chem.* **279**, 120910 (2019).
- [74] A. Durán, R. Escamilla, R. Escudero, F. Morales, and E. Verdín, Reversal magnetization, spin reorientation, and exchange bias in doped with praseodymium, *Phys. Rev. Mater.* **2**, 014409 (2018).
- [75] I. Fita, R. Puzniak, E. E. Zubov, P. Iwanowski, and A. Wisniewski, Temperature-driven spin switching and exchange bias in the ferrimagnet, *Phys. Rev. B* **105**, 094424 (2022).
- [76] A. Harres, M. Mikhov, V. Skumryev, A. M. H. d. Andrade, J. E. Schmidt, and J. Geshev, Criteria for saturated magnetization loop, *J. Magn. Magn. Mater.* **402**, 76 (2016).
- [77] R. Padam, S. Pandya, S. Ravi, S. Ramakrishnan, A. K. Nigam, A. K. Grover, and D. Pal, Study of the sign change of exchange bias across the spin reorientation transition in $\text{Co}(\text{Cr}_{1-x}\text{Fe}_x)_2\text{O}_4$ ($x = 0.00-0.125$), *J. Phys.: Condens. Matter* **29**, 055803 (2017).
- [78] L. Wang, L. L. Zhang, X. Zhang, M. L. Zhong, Z. C. Zhong, and G. H. Rao, Tunable reversals of magnetization and exchange bias of perovskite $\text{YbCr}_{1-x}\text{Fe}_x\text{O}_3$ ($x = 0-0.15$), *Ceram. Int.* **45**, 6143 (2019).
- [79] D. J. Webb, A. F. Marshall, Z. Sun, T. H. Geballe, and R. M. White, Coercivity of a macroscopic ferrimagnet near a compensation point, *IEEE Trans. Magn.* **24**, 588 (1988).
- [80] A. McDannald, C. R. dela Cruz, M. S. Seehra, and M. Jain, Negative exchange bias in single-phase $\text{Dy}_{1-x}\text{Nd}_x\text{CrO}_3$ induced by Nd doping, *Phys. Rev. B* **93**, 184430 (2016).
- [81] B. Maji, M. K. Ray, K. G. Suresh, and S. Banerjee, Large exchange bias and magnetocaloric effect in TbMn_2Si_2 , *J. Appl. Phys.* **116**, 213913 (2014).
- [82] M. K. Sharma, K. Singh, and K. Mukherjee, Exchange bias in a mixed metal oxide based magnetocaloric compound $\text{YFe}_{0.5}\text{Cr}_{0.5}\text{O}_3$, *J. Magn. Magn. Mater.* **414**, 116 (2016).
- [83] J. R. Jesus, F. Garcia, J. G. S. Duque, and C. T. Meneses, Study of exchange bias in single-phase $\text{Dy}_{0.2}\text{Nd}_{0.8}\text{CrO}_3$, *J. Alloys Compd.* **779**, 577 (2019).
- [84] X. X. Zhang, Z. C. Xia, Y. J. Ke, X. Q. Zhang, Z. H. Cheng, Z. W. Ouyang, J. F. Wang, S. Huang, F. Yang, Y. J. Song *et al.*, Magnetic behavior and complete high-field magnetic phase diagram of the orthoferrite ErFeO_3 , *Phys. Rev. B* **100**, 054418 (2019).
- [85] C. Ritter, R. Vilarinho, J. A. Moreira, M. Mihalik, M. Mihalik, and S. Savvin, The magnetic structure of DyFeO_3 revisited: Fe spin reorientation and Dy incommensurate magnetic order, *J. Phys.: Condens. Matter* **34**, 265801 (2022).
- [86] T. Yamaguchi and K. Tsushima, Magnetic symmetry of rare-earth orthochromites and orthoferrites, *Phys. Rev. B* **8**, 5187 (1973).
- [87] T. Nakajima, Y. Tokunaga, Y. Taguchi, Y. Tokura, and T.-H. Arima, Piezomagnetolectric effect of spin origin in dysprosium orthoferrite, *Phys. Rev. Lett.* **115**, 197205 (2015).